Journal of Power and Energy Engineering, 2021, 9, 1-32
https://www.scirp.org/journal/jpee
ISSN Online: 2327-5901
ISSN Print: 2327-588X

Effect of Mn on the Performance and Mechanism of Catalysts for the Synthesis of $(Ce,La)CO_3F$

Zedong Cheng[1], Na Li[1,2], Liming Hou[3], Kunling Jiao[1,3], Wenfei Wu[1,3*]

[1]Department of Energy and Environment, Inner Mongolia University of Science and Technology, Baotou, China
[2]Department of Environmental Science and Engineering, North China Electric Power University, Baoding, China
[3]Key Laboratory of Efficient and Clean Combustion, Inner Mongolia Autonomous Region, Baotou, China
Email: *wwf@imust.edu.cn

How to cite this paper: Cheng, Z.D., Li, N., Hou, L.M., Jiao, K.L. and Wu, W.F. (2021) Effect of Mn on the Performance and Mechanism of Catalysts for the Synthesis of $(Ce,La)CO_3F$. *Journal of Power and Energy Engineering*, **9**, 1-32.
https://doi.org/10.4236/jpee.2021.911001

Received: August 17, 2021
Accepted: November 14, 2021
Published: November 17, 2021

Abstract

In accordance with the cerium-lanthanum ratio of fluorocerium ores in the mineralogy of the Baiyun Ebo process, the $(Ce,La)CO_3F$ grains were synthesised by hydrothermal method using pure material to simulate bastnaesite minerals, and used as NH_3-SCR denitrification catalysts. The activity results showed that the synthetic $(Ce,La)CO_3F$ was roasted at 500˚C, and the NOx conversion was 27% at 200˚C. The NH_3-SCR catalytic activity of the synthesised $(Ce,La)CO_3F$ was improved by loaded transition metal Mn. The best catalyst was found to be produced by impregnating $(Ce,La)CO_3F$ with 1 mol/L manganese nitrate solution, with a NOx conversion of 80% at 250˚C. The loading of Mn resulted in the appearance of numerous well-dispersed MnOx species on the catalyst surface, the dispersion of Ce_7O_{12} species was also greatly enhanced, and the reduction in grain size indicated that Mn^{n+} entered into the $(Ce,La)CO_3F$ lattice causing lattice shrinkage. The number of acidic sites on the catalyst surface and the redox capacity were enhanced. The amount of Ce^{3+} in the catalyst was also enhanced by the introduction of Mn^{n+}, but the proportion of adsorbed oxygen decreased, which indicated that the introduction of Mn^{n+} was detrimental to the increase in the proportion of adsorbed oxygen. The reaction mechanisms of the $(Ce,La)CO_3F$ and $Mn/(Ce,La)CO_3F$ catalysts were investigated by *in-situ* Fourier transform infrared spectroscopy (FTIR). The results showed that catalysts followed the E-R and L-H mechanisms. When loaded with Mn, the main reactive species in the L-H mechanism were the NH_4^+ (ad) species on the Brønsted acidic site and the $O\text{-}Ce^{3+}\text{-}O\text{-}NO$, $O\text{-}Mn^{3+}\text{-}O\text{-}NO$ species. The main reactive species for the E-R mechanism were NH_3/ NH_4^+ (ad) species and NO. The NH_4^+ (ad) species on the Brønsted acidic sites act as the main reactive NH3 (g) ad-

sorbing species, bonded to the Ce^{4+} in the carrier $(Ce,La)CO_3F$ to participate in the acid cycle reaction. The introduction of Mn^{n+} increases the number of Brønsted acidic sites on the catalyst surface, and acts as an adsorption site for NO, to react with NO to generate more monodentate nitrate species, to participate in the redox cycle reactions. The above results indicated that Mn^{n+} and $(Ce,La)CO_3F$ have a good mutual promotion effect, which makes the loaded catalyst have excellent performance, which provides a theoretical basis for the high value utilization of bastnaesite.

Keywords

Synthesis of $(Ce,La)CO_3F$, Load, Denitrification Performance, Reaction Mechanism

1. Introduction

In recent years, domestic coal consumption has tended to increase and the air pollution problem caused by the coal combustion process has become increasingly serious, with coal-fired power plants representing 60% of the overall emissions from stationary sources. The use of coal, diesel and petrol to produce NOx can lead to a range of environmental problems, so NOx removal and reduction is imperative. SCR technology (Selective Catalytic Reduction) is now favoured by many researchers in the field of denitrification. The traditional V_2O_5-$WO_3(MoO_3)/TiO_2$ catalyst has not yet been solved due to its toxicity and narrow denitration temperature window, which has led to the research of new catalysts. Mineral catalysts have received increased attention from scholars due to their non-toxicity and wide range of elements.

The main rare-earth minerals in Baiyun Ebo rare-earth concentrates are bastnaesite, and the main rare-earth elements in rare-earth concentrates are Ce, La, Nd and Pr [1], of which cerium has a very efficient and promising future as a mineral catalytic material. However, the composition of rare earth concentrates is complex and the available characterisation tools have no way of determining the specific reaction changes of a multi-phase component catalyst. Exploring its specific reaction mechanism as a catalyst is also a blind spot that is difficult to break through, so we need to look at the mineral phases that play a catalytic role in the concentrate on a case-by-case basis and explore their denitrification mechanisms. As the main mineral phase in rare earth concentrates, the study of bastnaesite is necessary. The present technical means cannot extract the more pure bastnaesite, but there are many scholars who use the pure material to synthesise the mineral to study its properties. Huang Shunhua *et al.* [2] synthesised bastnaesite by hydrothermal method. Experimental results showed that from room temperature to 400˚C, atmospheric pressure to 100 MPa, the solution pH from 6.7 to 11.0 range as long as the necessary substances to form the mineral can be synthesized bastnaesite. The molecular formula of bastnaesite is

$(Ce,La)CO_3F$ according to the mineralogy of the Baiyun Ebo rare earth concentrate process, and the $(Ce,La)CO_3F$ crystals were prepared by the hydrothermal method of analytical purity.

The roasting of $(Ce,La)CO_3F$ produced Ce_7O_{12} species, which had poor performance as denitrification catalysts due to its good crystallinity, so the catalytic performance of $(Ce,La)CO_3F$ was promoted by introducing the transition metal Mn to improve the dispersion of Ce_7O_{12} species, as well as generating new active components. Cerium-based catalysts have excellent low-temperature catalytic performance, and many researchers have used CeO_2 as a carrier to improve the performance of NH_3-SCR. Solid oxide catalysts are sourced for due to their advantages ranging from low cost, recoverability and reusability, environmental benign-ness, thermal stability and high quality product generation [3]. Yao Xiaojiang [4] prepared a series of $MnOx/CeO_2$ catalysts by adjusting the solvents (deionised water, anhydrous ethanol, acetic acid, oxalic acid solution). The $MnOx/CeO_2$ catalysts prepared with oxalic acid solution as the solvent showed over 80% NO conversion in the range of 100˚C - 250˚C, and good low temperature sulphur and water resistance, probably because the solvent oxalic acid enhanced the electronic interaction between MnOx and CeO_2 and increased the oxygen vacancies in the carrier CeO_2, which can promote the decomposition of NO species. Therefore, this paper is used to improve the catalytic performance of $(Ce,La)CO_3F$ by loaded Mn, and to study its NH_3-SCR physicochemical properties and reaction mechanism by characterization and in-situ infrared, to clarify the specific reaction mechanism within bastnaesite, and to provide theoretical guidance for the reaction performance and mechanism of rare earth mineral catalysts.

2. Experimental Methods

2.1. Experimental Materials

Reagents used in the experiments, $Ce(NO_3)_3{\cdot}6H_2O$ (mass fraction), analytical purity, Tianjin Comio Chemical Reagent Co. $La(NO_3)_3{\cdot}6H_2O$ (mass fraction), analytical purity, Tianjin Comio Chemical Reagent Co. $NaHCO_3$, analytical purity, Tianjin Windship Chemical Reagent Technology Co. NaF, analytical purity, Tianjin Windship Chemical Reagent Technology Co. $Mn(NO_3)_2$, analytical purity, Shanghai Zhangyun Chemical Co.

2.2. Preparation of Catalyst

The synthesis of $(Ce,La)CO_3F$ was carried out by hydrothermal method. A certain amount of $Ce(NO_3)_3{\cdot}6H_2O$, $La(NO_3)_3{\cdot}6H_2O$, NaF, $NaHCO_3$ was placed in 100 ml of PTFE liner at room temperature. Then 80 ml of distilled water was poured into the PTFE liner with constant stirring, and the PTFE liner was placed into an autoclave under atmospheric pressure and 120˚C with stirring and heating for 2 h for hydrothermal reaction. After cooling, the mixture was filtered and dried at 80˚C to obtain synthetic $(Ce,La)CO_3F$. After cooling, the mixture was

filtered and dried at 80˚C to obtain synthetic (Ce,La)CO_3F. $Mn(NO_3)_2$ was dissolved in deionised water using the impregnation method and continuously stirred to form manganese nitrate solutions at concentrations of 0.2 mol/L, 0.4 mol/L, 0.6 mol/L, 0.8 mol/L and 1.0 mol/L, respectively. The synthetic (Ce,La)CO_3F was used as a carrier and poured into different concentrations of $Mn(NO_3)_2$ solution, sonicated for 2 h, left overnight, filtered and dried the suspension, and then roasted in a muffle furnace at 500˚C for 2 h. The solid material obtained was the Mn/(Ce,La)CO_3F catalytic material.

2.3. Experimental Procedure

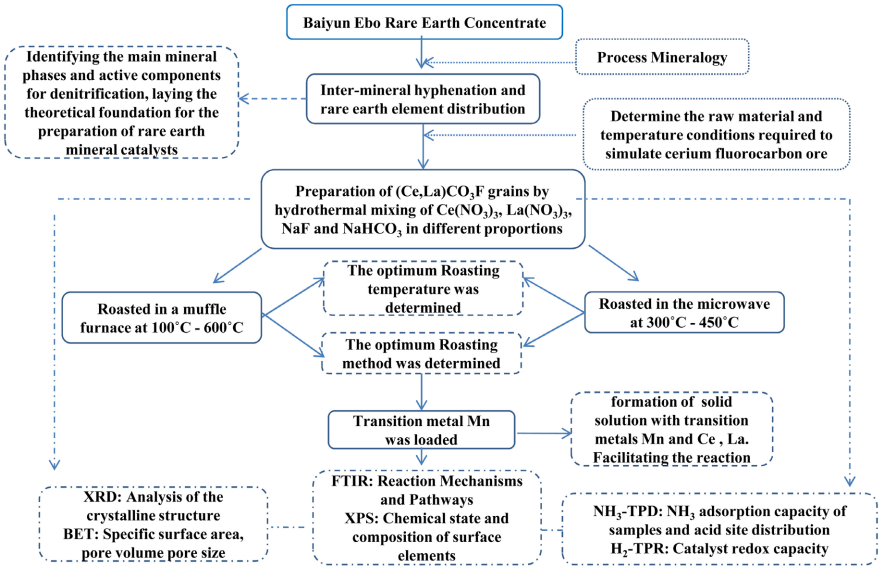

2.4. Testing of Catalytic Performance

The experiments were carried out in a reaction apparatus with quartz tubes for testing the activity of the catalyst NH_3-SCR. The reaction apparatus consists of a gas mixing tank-flow meter, standpipe furnace, quartz tube, Fourier infrared spectroscopy flue gas analyser and computer data acquisition system. The standpipe furnace was heated by a silicon-molybdenum rod model 1800 with a rated temperature of 1600˚C and an internal diameter of 20 mm and a length of 1.2 m from Nanjing Boynton Instrument Technology Co. The Fourier infrared spectroscopy (FTIR) flue gas analyser and data acquisition system were manufactured in Finland, and the model number was GASMET-DX4000. The simulated gas components were as follows: NH_3 500 ppm, NO 500 ppm, O_2 at a volume fraction of 6% of the total, N_2 as the equilibrium gas, a total gas flow of 100 ml/min, an air velocity of approximately 8000 $h^{-1}{\cdot}g^{-1}$ and a catalyst dosage of 0.6 g for each test.

3. Results and Discussion

3.1. Catalytic Performance Tests

Figure 1 showed the NOx conversion and N_2 selectivity of the Mn/(Ce,La)CO_3F

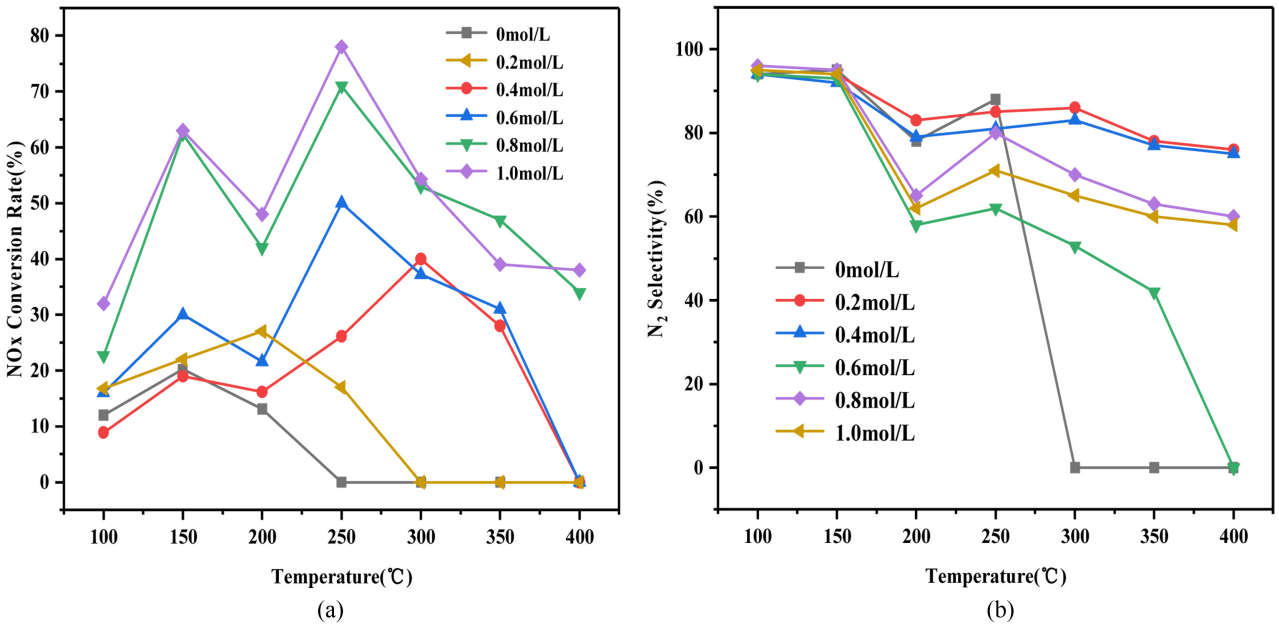

Figure 1. NOx conversion over catalyst (a) N_2 selectivity (b). (Reaction conditions 500 ppm NO, 500 ppm NH_3, 6% O_2, N_2 as balance gas).

catalysts obtained with Mn loaded. From the denitrification activity results, it can be seen that the NOx conversion of the Mn/(Ce,La)CO_3F catalysts with different loadings all increased with temperature in the temperature range of 100˚C - 150˚C, but as the temperature continued to be increased, the NOx conversion started to decrease at 200˚C and then increased again at 250˚C to reach the highest value for the whole catalytic reaction.

The reason for this may be due to the large amount of NO adsorbed on the catalyst surface in the range of 100˚C - 150˚C, which reduces the value of NOx, but NOx is not being reacted on the catalyst surface at this point, merely occupied as an active site, and as NO continues to pass through, NO cannot continue to be adsorbed, due to the absence of active sites on the catalyst surface. It is not until 250˚C that the NH_3-SCR reaction on the catalyst surface begins to take place, allowing the catalyst to reach maximum denitrification efficiency. It may also be due to the activation of species by adsorption of NH_3 and NO on the catalyst surface. That is to say, NH_3/ NH_4^+ and species such as NO_2, nitrate and nitrite are less stable on the catalyst surface and are particularly susceptible to temperature, decomposing at 200˚C, which leads to a decrease in activity. It can be found that when (Ce,La)CO_3F is impregnated in a 1 mol/L solution of $Mn(NO_3)_2$, the conversion of catalyst NOx can reach 80% at 250˚C. However, as the temperature continued to increase, the conversion rate also gradually decreased, which may be due to the oxidation of the reducing agent NH_3, which resulted in a decrease in the amount of reducing agent, and the oxidation of NH_3 at high temperature would release NO, which increased the concentration of NO but decreased the conversion rate. **Figure 1(b)** showed the N_2 selectivity graphs for the synthesis of (Ce,La)CO_3F as well as (Ce,La)CO_3F loaded with Mn. N_2 se-

lectivity is another important indicator to evaluate denitrification performance. In the NH_3-SCR denitrification process, side reactions such as oxidation of ammonia and high temperature decomposition of nitrate and ammonium nitrogen lead to partial production of N_2O, which greatly reduces the N_2 selectivity. From Figure 1(b) it can be obtained that when loaded with the transition metal Mn, the N_2 selectivity of the catalyst starts to decrease after 150˚C, which is related to the excessive hydrogen capture due to the strong redox ability of Mn^{n+}.

3.2. Physical Phase Structure Analysis

Figure 2 showed XRD diagrams of the synthetic (Ce,La)CO_3F catalyst roasted at 200˚C -600˚C in a muffle furnace. As can be seen in Figure 2, at 200˚C most of the $CeCO_3F$, $LaCO_3F$ and (Ce,La)CO_3F do not decompose, but the degree of crystallinity and dispersion is greatly improved and many of the diffraction peaks are significantly reduced.

At 300˚C the diffraction peaks of species such as $CeCO_3F$ and $LaCO_3F$ are further reduced and some decomposition occurs. The decomposition of $CeCO_3F$ gave rise to $Ce_{11}O_{20}$, Ce_6O_{11}, Ce_7O_{12} and CeF_3 species, and the decomposition of $LaCO_3F$ gave rise to LaCO, La_2O_3 and LaF_3 species, with the (Ce,La)CO_3F catalyst starting to decompose at 300˚C. At 400˚C, the most active stage of decomposition on the catalyst surface, $CeCO_3F$ and $LaCO_3F$ species were completely decomposed, with only a few species in amorphous form on the catalyst surface, and a large amount of $CeCO_3F$ decomposed into $Ce_{11}O_{20}$ and Ce_6O_{11} species, and Ce_7O_{12} species increased significantly compared to 300˚C. The main diffraction

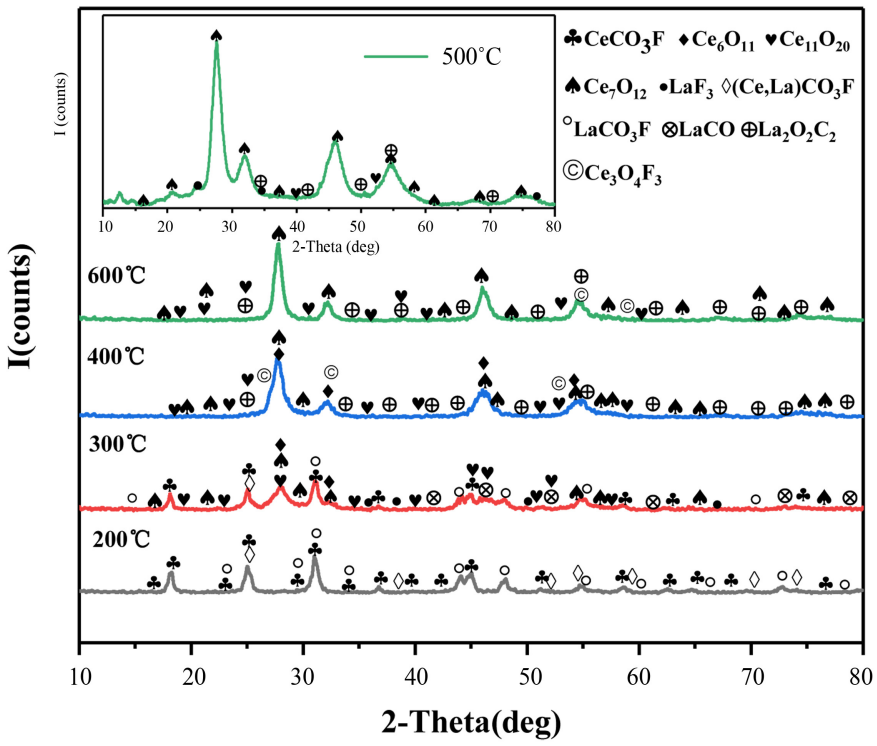

Figure 2. XRD patterns of (Ce,La)CO_3F after roasting at different temperatures.

peaks were mostly a composite of Ce_7O_{12} and Ce_6O_{11} species, both of which were formed under very similar conditions. The 500˚C roasting condition is the most stable stage for the catalyst surface species, and the main diffraction peaks of the catalyst are all Ce_7O_{12} species, while $LaCO_3F$ is present as $La_2C_2O_2$, with some CeF_3 and LaF_3 species also present. Combined with the activity tests at different roasting temperatures, the best denitrification effect was obtained after roasting at 500˚C. Therefore, combined with the XRD pattern at 500˚C, it can be seen that the Ce_7O_{12} species is the main active component of the reaction, which is more favourable to interact with other substances to promote the reaction than the $Ce_{11}O_{20}$ and Ce_6O_{11} species. At 600˚C, the Ce_7O_{12} species on the catalyst surface decreased and $Ce_{11}O_{20}$ and Ce_6O_{11} species gradually appeared, so there was a relative decrease in the active component, perhaps due to the change in catalyst structure caused by the high roasting temperature, which was not conducive to the reaction.

Figure 3 showed the XRD patterns of Mn loaded by the over-impregnation method. From Figure 3, it can be seen that the diffraction peaks of Ce_7O_{12} were dominated on the catalyst surface, accompanied by some CeO_2 species produced after roasting, and CeOF species. The diffraction peaks of Ce_7O_{12} species on the catalyst surface decreased gradually with increasing loading. Indicated that the addition of manganese nitrate can cause more cracks and oxygen vacancies on the surface of the carrier, which is conducive to improving the dispersion of the active components on the surface of the carrier, and Mn can interact with Ce and La in the synthetic $(Ce,La)CO_3F$ to reduce the crystallinity and increase the specific surface area. The $La_2O_2C_2$ species also showed some improvement in

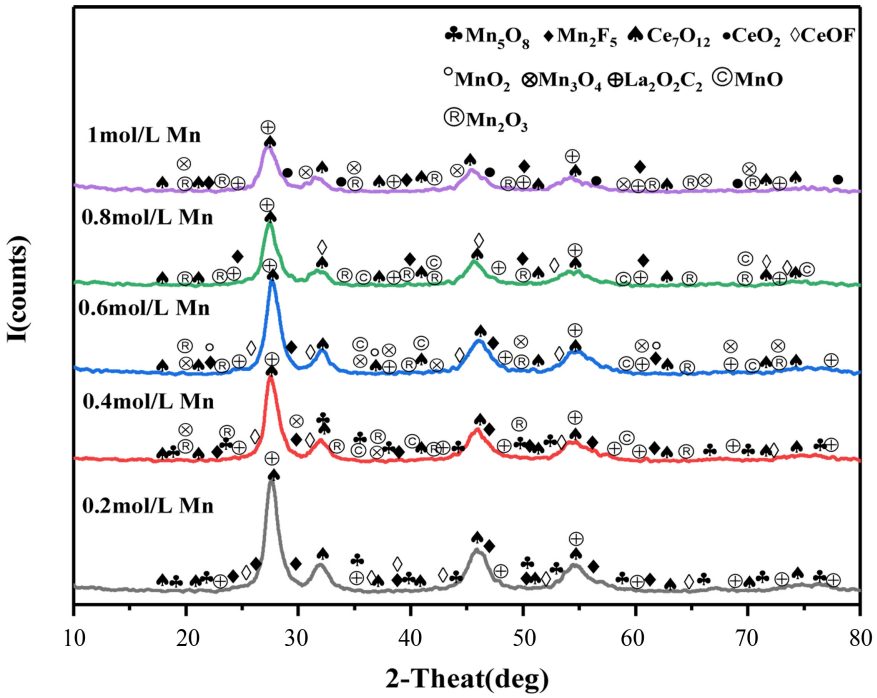

Figure 3. XRD patterns of loaded Mn.

dispersion with increasing Mn loading, and from the figure, MnOx species such as Mn_3O_4, Mn_2O_3, MnO_2 and MnO can also be observed. There were more MnOx species on the 0.8 mol/L and 1 mol/L catalysts compared to the less loaded catalysts. The presence of MnOx species is beneficial to the improvement of catalytic oxidation reduction, and the dispersion of MnOx species on the catalyst gradually became better, mainly in amorphous form on the catalyst surface, and the amorphous structure was favourable to the improvement of catalytic performance [5]. Due to the multiple valence states of Mn^{n+}, the interconversion of manganese ions facilitates the redox performance of the catalyst as well as the oxygen migration, both of which are beneficial for the conversion of NO to NO_2. Generally speaking too high a loading will lead to a decrease in NO removal, this is because the dispersion of the transition metal in the catalyst starts to decrease, which leads to a conversion of the active material in the catalyst from an amorphous form to a crystalline form. It can be found that the highest catalytic activities of the catalysts with 0.8 mol/L and 1 mol/L Mn loading amounts are similar and basically close to each other. This indicates that the dispersion of Mn within the catalyst has tended to decrease. However, due to the poor redox and NH_3 adsorption capacity of synthetic $(Ce,La)CO_3F$, the synthetic $(Ce,La)CO_3F$ can be loaded with more Mn than other carriers and maintain a stable denitrification effect. It can also be observed from the figure that composite peaks of Ce_7O_{12} species and MnOx species appear at 36.8˚, 38.5˚ and 55˚ in a companion relationship, which indicates that a Mn-Ce solid solution may have formed on the catalyst surface. In support of this conclusion, calculations of the cell constants were carried out for the Mn-loaded catalysts and the results are shown in Table 1. Compared with the synthesis of $(Ce,La)CO_3F$, the crystal plane spacing and grain size of the catalyst decreased after loading Mn, and it was not until the crystal plane spacing increased that the surface structure of $Mn/(Ce,La)CO_3F$ was the most stable. The decrease in lattice parameters indicates that some of the Mn^{n+} has entered the lattice of $(Ce,La)CO_3F$ to form a Mn-Ce-La solid solution, due to the ionic radii of Mn^{n+} being Mn^{2+} (0.65 Å), Mn^{3+} (0.58 Å), Mn^{4+} (0.53 Å), and Ce^{n+} being Ce^{4+} (0.97 Å), Ce^{3+} (1.14 Å), and La^{3+} (1.16 Å) in $(Ce,La)CO_3F$. Since the ionic radii of Mn^{n+} are all smaller than Ce and La ions, the smaller ionic radii can replace the larger ones. When Ce^{4+} (0.97 Å), Ce^{3+} (1.14 Å) and La^{3+}

Table 1. Cell constants of catalysts.

catalysts	Grain spacing D (nm)	Grain size
$(Ce,La)CO_3F$	5.014	280
Mn(0.2 mol/L)/$(Ce,La)CO_3F$	4.552	160
Mn(0.4 mol/L)/$(Ce,La)CO_3F$	4.486	168
Mn(0.6 mol/L)/$(Ce,La)CO_3F$	4.486	164
Mn(0.8 mol/L)/$(Ce,La)CO_3F$	4.389	154
Mn(1.0 mol/L)/$(Ce,La)CO_3F$	4.345	142

(1.16 Å) are replaced by Mn^{n+} with smaller ionic radii, it will lead to changes in the lattice parameters. In addition, the grain size of Mn-doped $(Ce,La)CO_3F$ is much smaller than when undoped due to the formation of Mn-Ce-La solid solution, which inhibits grain growth and causes lattice shrinkage, making the grain size smaller. It has also been reported in the literature that the formation of the Ce-M (metal ion)-O solid solution can inhibit the growth of metal oxide crystals and promote the activation of oxygen species, thus accelerating the NH_3-SCR reaction [6].

3.3. Specific Surface Area Analysis

Figure 4(a) and **Figure 4(b)** showed the isothermal curves of N_2 adsorption-desorption for different catalysts respectively, and **Table 2** showed the specific surface area, pore capacity and pore size of each catalyst.

From **Figure 4(a)** it can be seen that the synthetic $(Ce,La)CO_3F$ catalysts exhibit a type II adsorption-desorption isotherm curve, such that the curve often occurs on non-porous solid surfaces or on macroporous solids free of a single

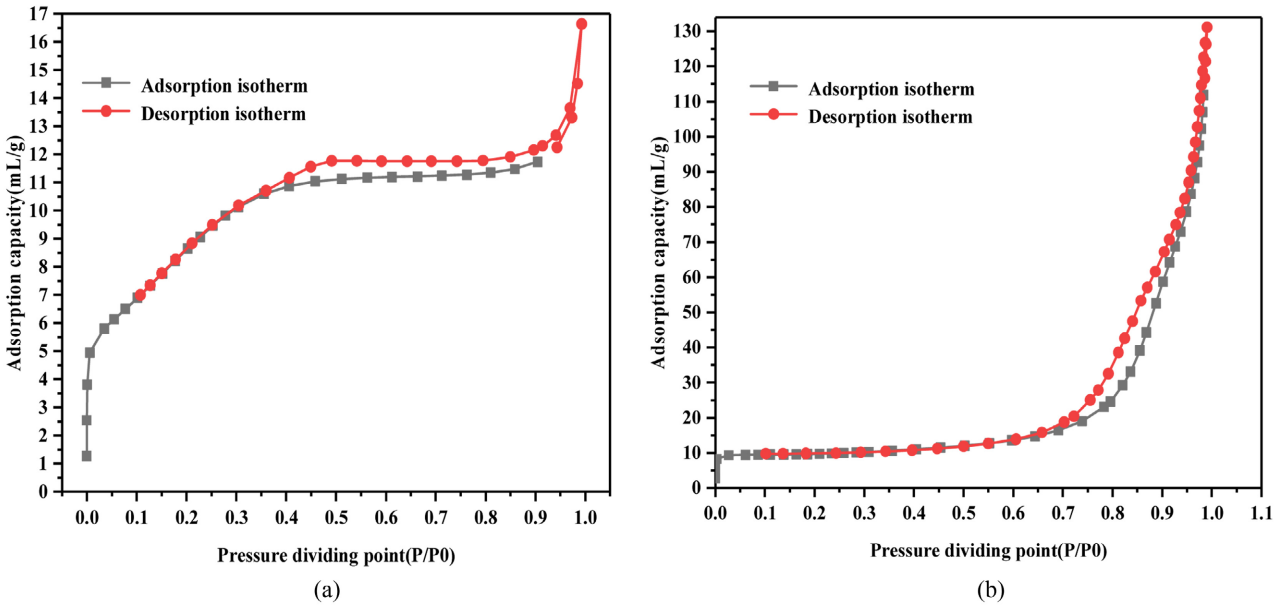

Figure 4. Adsorption-desorption isotherm profile of the catalyst. (a) $(Ce,La)CO_3F$; (b) Mn(1.0 mol/L)/$(Ce,La)CO_3F$.

Table 2. Catalyst specific surface area data.

Catalysts	BET surface area (m^2/g)	Pore volume (cm^3/g)	Pore diameter (nm)
$(Ce,La)CO_3F$	50.32	0.1746	21.7867
Mn(0.2 mol/L)	44.56	0.1788	22.3824
Mn(0.4 mol/L)	43.72	0.1847	22.4263
Mn(0.6 mol/L)	43.87	0.1875	22.7875
Mn(0.8 mol/L)	45.83	0.1986	24.4689
Mn(1.0 mol/L)	45.41	0.2034	26.4853

multilayer reversible adsorption process. The curve is characterised by an inflection point at low P/P0, the first steep part of the isotherm, which indicated the saturated adsorption capacity of the monomolecular layer, and from **Figure 4(a)** it can be concluded that synthetic (Ce,La)CO_3F has a poor adsorption capacity at low pressures. However, as the relative pressure increases, a second layer begins to form, and at saturation vapour pressure the number of adsorption layers is infinite, which also indicated a larger increase in adsorption capacity. The type II isotherm, commonly encountered at adsorbent pore sizes greater than 20 nm, has no upper limit to the solid pore size. In the low P/P0 region, the convex upward curve reflects a stronger interaction between the adsorbent and the adsorbate. In contrast, after doping with Mn, as shown in **Figure 4(b)**, the Mn/(Ce,La)CO_3F catalyst exhibits a Type III adsorption-desorption isotherm curve, which can be found to have no inflection point in the entire pressure range, and is convex downwards, often presenting this type when the adsorption interaction between the solid and the adsorbate is smaller than the interaction between the adsorbates. The small amount of adsorption in the low pressure region, and the absence of an inflection point, indicated that the forces between the adsorbent and the adsorbate were rather weak. The higher the relative pressure, the higher the adsorption amount, which showed a pore filling, which indicated that (Ce,La)CO_3F has a rich pore structure when used as a carrier, which facilitates the entry and exit of the loaded metal ions and the reaction gas. As can be seen from **Table 2**, the physical structure of the carrier is affected by the loaded of the active component, and the specific surface area of the catalysts all decreased after loaded with the transition metal Mn, while the pore capacity and pore size increased. It has been reported in the literature that the pore size of the catalyst is in the mesoporous range, and that an appropriate increase in the pore radius of the catalyst facilitates the adsorption and desorption of the reacting gas molecules at the active sites on the catalyst surface, thus being more conducive to the catalytic reaction [7]. The increase in pore volume pore size is also due to the interaction of Mn, Ce and La to promote dispersion of each other, and facilitate the entry and exit of the reaction gases. However, it can also be found that the Mn/(Ce,La)CO_3F catalyst made by impregnation in a 1 mol/L manganese nitrate solution has the best denitrification effect but not the largest specific surface area, which indicated that the specific surface area is only one of the factors affecting the catalytic activity and is not the main reason [8].

3.4. Redox and Adsorption and Desorption Performance Analysis

Figure 5(a) showed the NH_3-TPD diagram of Mn/(Ce,La)CO_3F catalyst obtained after ultrasonic impregnation of Mn loaded at different concentrations. Firstly, it can be seen from **Figure 5(a)** that the catalysts obtained by impregnation with 0.4 mol/L and 0.6 mol/L manganese nitrate solutions showed a similar trend in the desorption peak of NH_3, and the catalysts obtained by impregnation with 0.8 mol/L and 1.0 mol/L manganese nitrate solutions have similar peak positions. Usually the binding of NH_3 to the Brønsted acid site and the weak Lewis

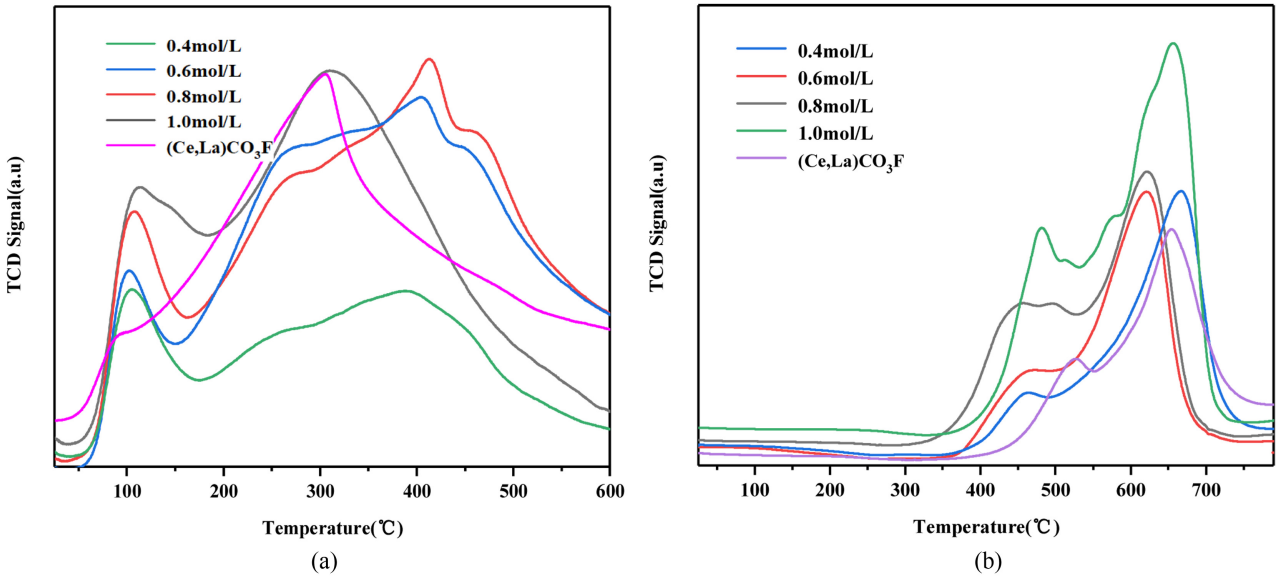

Figure 5. NH_3-TPD (a) H_2-TPR (b) with different ratios of loaded Mn.

acid site is around 200˚C. The desorption peaks in the 400˚C range are caused by the desorption of ammonia at the moderately acidic site and the 500˚C peak is caused by the binding of ammonia to the strong Lewis acid site [9] [10]. The graph showed that the (Ce,La)CO_3F sample showed a shoulder peak near 93˚C, where the desorption peak belonged to the binding of NH_3 to the weak Brønsted acidic site, and at 312˚C, where the peak belonged to the binding of NH_3 to the Brønsted acidic site and the medium Lewis acidic site. The Mn-loaded catalysts all showed a strong NH_3 desorption peak at around 100˚C. The Mn-loaded catalysts all showed a strong NH_3 desorption peak at around 100˚C. The desorption peak that appeared here belonged to the desorption of NH_3 from the physisorbed state on the weak acidic sites and the dissociation of the Brønsted acidic sites, possibly accompanied by the binding to the weak Lewis acidic sites [11], Which indicated that the loading of the transition metal Mn increased the activity of the Brønsted acidic sites on the catalyst surface, number of acidic sites, resulting in increased activity in the low temperature section.

The NH_3 desorption peak at 310˚C for the catalyst impregnated in 0.6 mol/L solution belonged to the strong adsorption of NH_3 on the Brønsted acidic site and the moderate adsorption on the Lewis acidic site. The other three Mn-loaded catalysts all showed NH_3 desorption peaks within 390˚C - 460˚C. Here the desorption peaks were caused by the combination of NH_3 and moderate Lewis acidic sites [10], which indicated that the addition of the manganese nitrate solution resulted in a greater abundance of acidic sites on the catalyst surface. The peak area is generally considered to indicate the number of acidic sites. From **Table 3**, it can be obtained that the peak area gradually increased with the increase of loading, which indicated that the adsorption capacity of NH_3 gradually increased, which was consistent with the activity test results. It is not difficult to find that the adsorption capacity of NH_3 on the catalyst surface was

Table 3. Peak areas of NH_3-TPD adsorption and desorption curves.

catalysts	Peak temperature (T/˚C)	Peak area
$(Ce,La)CO_3F$	93, 312	2031.3
Mn(0.4 mol/L)/$(Ce,La)CO_3F$	102, 391	590.96
Mn(0.6 mol/L)/$(Ce,La)CO_3F$	114, 310	1169.18
Mn(0.8 mol/L)/$(Ce,La)CO_3F$	100, 408, 458	1433.14
Mn(1.0 mol/L)/$(Ce,La)CO_3F$	105, 415, 464	1443.26

significantly enhanced when Mn elements were introduced into the synthetic $(Ce,La)CO_3F$, and the adsorption capacity also increased with increasing loading, which indicated that the enhancement of the adsorption performance originated from chemical action [12].

Figure 5(b) showed the H_2-TPR patterns of the $(Ce,La)CO_3F$ and Mn/$(Ce,La)CO_3F$ catalysts, From **Figure 5(b)**, it can be seen that the $(Ce,La)CO_3F$ catalyst showed a reduction peak at 521˚C, where the reduction peak is attributed to the reduction of Ce^{4+} to Ce^{3+} [13], and with the increase in temperature, the reduction peak at 651˚C which was attributed to the reduction of the catalyst bulk phase CeO_2 [14]. The oxide of La in $(Ce,La)CO_3F$ was La_2O_3, which also has a +2 valence state based on the arrangement of its outer electrons, and since La, Ce are neighbouring rare earth elements with relatively similar chemical properties, La may also have some redox ability. The catalysts loaded with Mn all showed reduction peaks at 450˚C - 490˚C. The reduction peaks here can be attributed to the process of $MnO_2/Mn_2O_3 \rightarrow Mn_3O_4 \rightarrow MnO$ conversion [15] [16], and due to the large number of MnOx species, the reaction process can be interconverted, which facilitates the redox reaction. The catalyst obtained by impregnation in a 0.4 mol/L solution, apart from the reduction of Mn^{n+} at 452˚C, the obvious change was the enhanced reduction of the bulk phase CeO_2 at 661˚C and promoted the reaction. With increased loading, the position of the reduction peak of the bulk phase CeO_2 shifted towards the low temperature section, and the H_2 adsorption also increased significantly, Which indicated that strong electronic interactions between the MnOx species on the catalyst surface and CeO_2 occurred, and the interactions promoted the reduction of Ce^{4+} on the surface. From **Table 4**, it can be seen the catalyst obtained by impregnation in 1.0 mol/L solution had the largest peak area compared to the other Mn-loaded catalysts, which indicated a higher redox capacity, the most active reduction of Ce^{4+} to Ce^{3+} under these conditions, the increase in the reduction potential of the active component, the formation of oxygen vacancies and more oxygen species, which facilitated the migration of oxygen and enhanced the activation reaction of the catalyst, and the catalyst has excellent redox ability.

3.5. Surface Element Valence Analysis

Figure 6(a) showed the Ce 3d spectrum. From **Figure 6(a)** it can be seen that

Table 4. Peak areas of H_2-TPR adsorption and desorption curves.

catalysts	Peak temperature (T/˚C)	Peak area
$(Ce,La)CO_3F$	521, 651	7320.32
Mn(0.4 mol/L)/$(Ce,La)CO_3F$	452, 661	7173.75
Mn(0.6 mol/L)/$(Ce,La)CO_3F$	456, 613	6978.59
Mn(0.8 mol/L)/$(Ce,La)CO_3F$	442, 489, 613	9725.08
Mn(1.0 mol/L)/$(Ce,La)CO_3F$	468, 571, 648	13,107.51

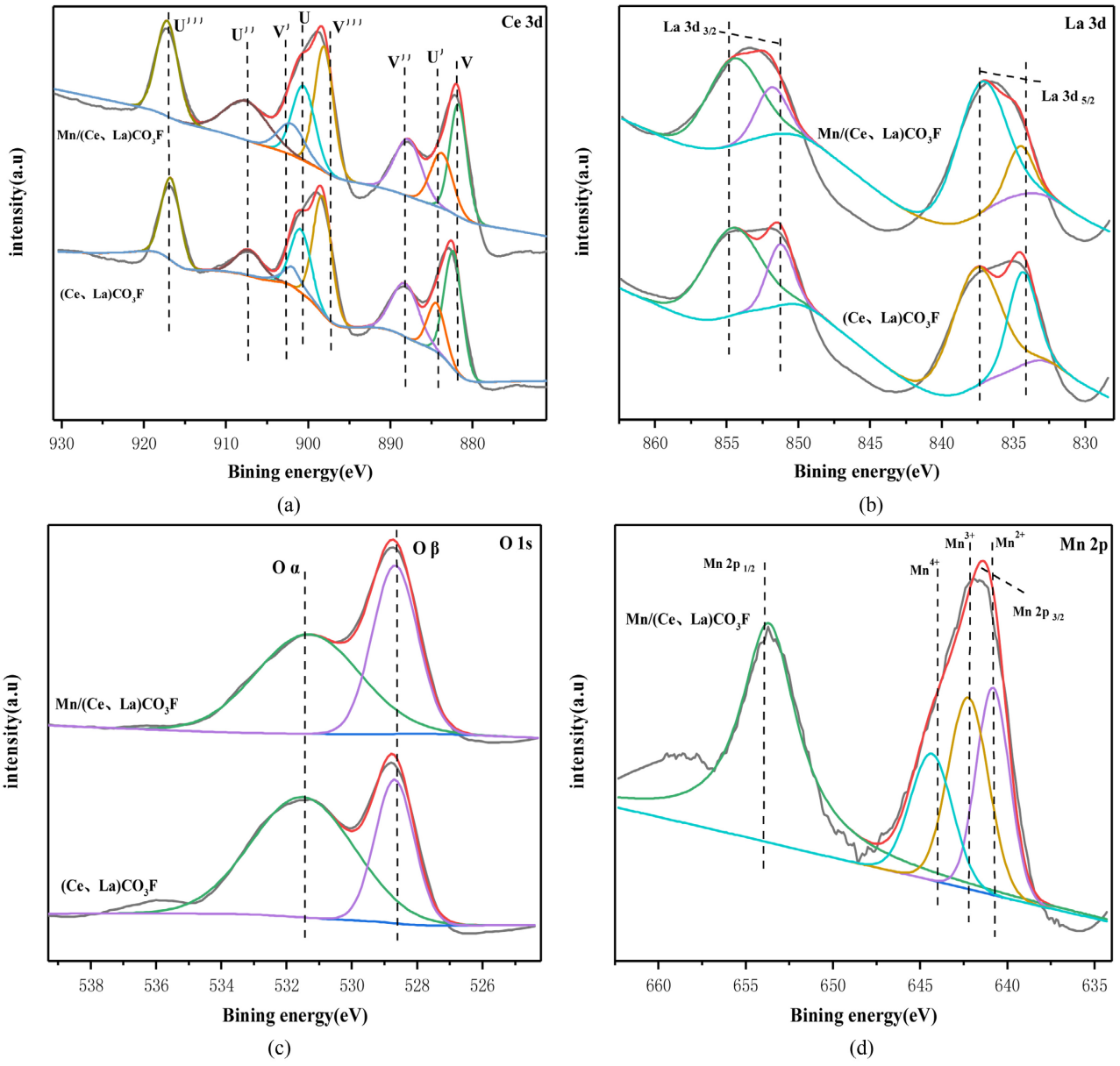

Figure 6. XPS with different catalysts.

the Ce 3d spectrum contains eight characteristic peaks. Of these, u (900.8 ev), u" (907.5 ev), u"' (916.5 ev), v (882.3 ev), v" (888.9 ev), v"' (898.4 ev) were attributed

to Ce^{4+}. u' (903.8 ev), v' (884.7 ev) had characteristic peaks that belonged to Ce^{3+} [17] [18]. It is obviously evident from **Figure 6(a)** that the Mn/(Ce,La)CO_3F catalyst has a stronger peak at u', v' compared to the (Ce,La)CO_3F catalyst, which implies an increased Ce^{3+} content on the catalyst surface. The higher $Ce^{3+}/(Ce^{4+}+Ce^{3+})$ ratio indicated that this catalyst exhibited an unsaturated chemical energy band and more oxygen vacancies, which would promote the adsorption of NH_3 from the reactant [19] [20] [21], which is consistent with the results of NH_3-TPD. The proportion of each type of element is calculated in **Table 5**, from which it can be obtained that by loading the transition metal Mn, the content of Ce^{3+} does increase compared to the original carrier, which indicated that the introduction of Mn^{n+} can cause Mn, Ce interaction, which makes part of Ce^{4+} to convert into Ce^{3+}, promoting the redox ability of each other, which is beneficial to the SCR reaction. The elevated content of Ce^{3+} is beneficial to promote the transfer of oxygen on the catalyst surface and the regeneration of the active site in the redox cycle reaction.

Figure 6(b) showed the La 3d spectrum with electron binding energies of magnitude 854 - 855 ev, 850 - 851 ev, 837 - 838 ev and 833 - 834 ev [22]. The characteristic peaks of lanthanum metal are double peaks. When lanthanum metal forms a composite oxide $La3d_{3/2}$ and $La3d_{5/2}$ appear as companion peaks. The reason for the appearance of the companion peaks was the ionisation of electrons in the inner shell layers of $La3d_{3/2}$ and $La3d_{5/2}$, and the transfer of 2p valence electrons from the ligand oxygen with La to the 4f vacant orbital of La, causing the splitting of the La3d characteristic peak, which leads to the result of the vibronic companion peaks of $La3d_{3/2}$ and $La3d_{5/2}$ [23] [24], where the binding energy in the La 3d pattern of the synthetic (Ce,La)CO_3F catalyst is lower than that of the standard characteristic peak and accompanying peaks. This indicated that there is no transfer of electrons between the metals La [25] and that a Ce-La-O solid solution may be formed here [26]. When loaded with the transition metal Mn, the electron binding energy of $La3d_{5/2}$ was shifted more towards the lower end, probably due to the introduction of a third metal, which enhanced the inter-elemental interactions forming a new solid solution (Mn-Ce-La), which is consistent with the XRD results.

Figure 6(c) showed the O 1s spectrum of catalyst. The peak at 531.3 ev belonged to the surface adsorbed oxygen species, denoted as Oα, and the peak at 529.5 ev belonged to the lattice oxygen species, denoted as Oβ [27]. As can be seen from **Figure 6(c)**, after loading with Mn, the lattice oxygen peak is slightly enhanced, but the adsorbed oxygen peak is weakened, but is similar to (Ce,La)CO_3F. The chemisorbed oxygen (Oα) is the most active oxygen species

Table 5. Fitted data of XPS on the catalyst.

samples	$Ce^{3+}/(Ce^{3+}+Ce^{4+})$(%)	$O_\alpha/(O_\alpha+O_\beta)$(%)	$Mn^{4+}/(Mn^{4+}+Mn^{3+}+Mn^{2+})$(%)
(Ce,La)CO_3F	10.7	71.12	-
Mn(1 mol/L)/(Ce,La)CO_3F	13.16	63.3	14.54

and plays a key role in the redox reaction [28]. From the calculations in **Table 5**, it can be seen that the (Ce,La)CO_3F catalyst itself contains more surface adsorbed oxygen, and after loading with transition metals, the proportion of adsorbed oxygen decreases, which is probably because the addition of Mn does not contribute to the increase of chemisorbed oxygen (Oα). (Ce,La)CO_3F and the catalyst after loading with the transition metal Mn, the binding energy of O 1s shifted slightly towards the lower compared to the standard binding energy. This suggested that O and the metal element interacted to form the Mn-O-Ce(La) species, which shifted to a lower binding energy due to its shorter bond length [29] [30].

Figure 6(d) showed the Mn 2p spectrum for the Mn/(Ce,La)CO_3F catalyst. From **Figure 6(d)**, the Mn 2p band can be obtained as two main peaks, Mn $2p_{1/2}$ (654.2 ev) and Mn $2p_{3/2}$ (641.1 ev). The Mn 2p of all catalysts can be further decomposed into three peaks, where the binding energy in the range of 641.0 - 641.3 ev belonged to Mn^{2+}, 642.0 - 642.6 ev to Mn^{3+} and 644.0 - 644.7 ev to Mn^{4+} [31]. It is generally accepted that the catalytic capacity of MnOx is MnO_2 > Mn_3O_4 > Mn_3O_4 [32] [33] [34] and that the catalyst surface produces a large amount of MnO_2 to facilitate the SCR reaction [35]. The reason why Mn^{4+} plays more of a role in the NH_3-SCR reaction than Mn^{3+} and Mn^{2+} is because its high redox ability can facilitate the conversion of NO to NO_2 and enhance the catalytic activity of the low temperature section through the fast SCR reaction: NO + NO_2 + $2NH_3$ = $3N_2$ + $2H_2O$, and therefore this reaction is also the main pathway for the low temperature reaction [36] [37].

4. *In-Situ* Infrared Analysis and Reaction Mechanism Study

In-Situ Infrared Spectroscopy of NH_3 and NO+O_2 Adsorption Stability on Catalyst Surfaces

In order to investigate the effect of catalyst activation by NH_3 adsorption at optimum temperature conditions, in-situ IR spectroscopy was carried out on (Ce,La)CO_3F and the catalysts produced after loading with Mn. From the activity test results, it was found that (Ce,La)CO_3F reached the optimum activity at 200˚C, and Mn(1 mol/L)/(Ce,La)CO_3F reached the optimum denitrification efficiency at 250˚C. This experiment investigated the variation of NH_3 adsorption over time for both catalysts at the optimum denitrification temperature. **Figure 7(a)** showed the infrared spectra of NH_3 with time for the synthetic (Ce,La)CO_3F. From the figure, it can be seen that two distinct infrared absorption peaks appeared at 1590 cm^{-1} and 1301 cm^{-1} after 5 min of NH_3 passage, the absorption peak at 1590 cm^{-1} was attributed to the NH_3 species in the ligand state on the Lewis acidic site [38], and the absorption peak at 1301 cm^{-1} is attributed to the dehydrogenation product eNH_2 produced by the dehydrogenation reaction of the activated NH_3 species [39]. With increased passage time of NH_3, the NH_3 species adsorbed at the Lewis acidic site at 1590 cm^{-1} disappeared at 10 min, which indicated that it was very unstable with time. At 20 - 30 min pass,

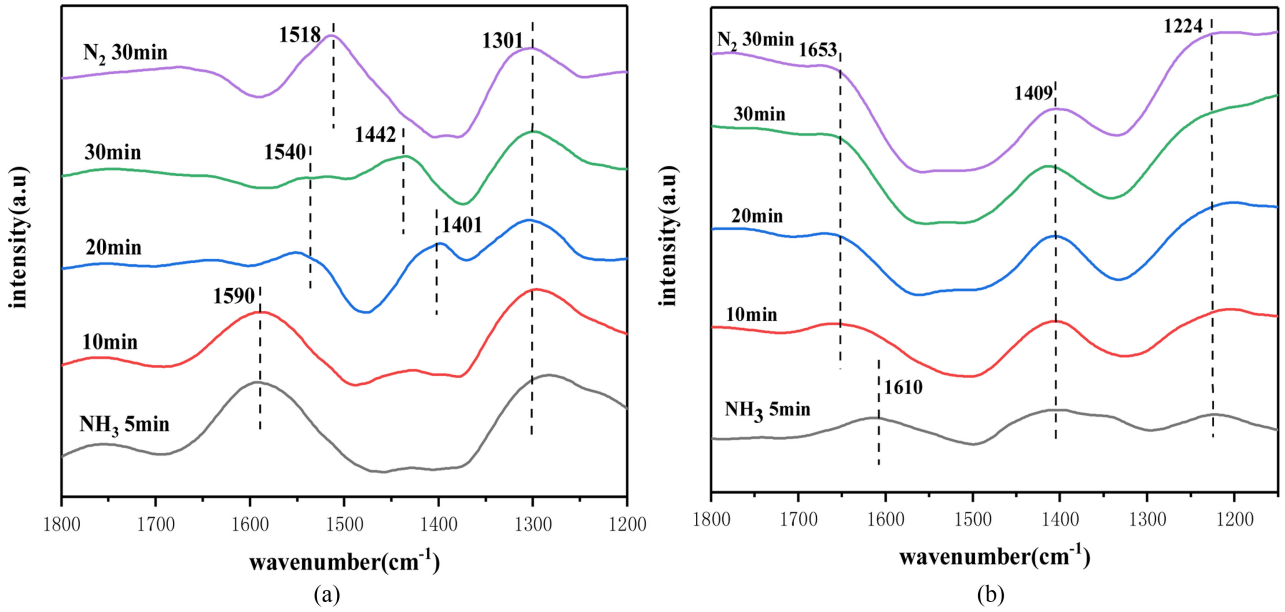

Figure 7. *In-situ* infrared spectra of NH_3 adsorption of the catalyst at the optimal denitration temperature over time. (a) $(Ce,La)CO_3F$. (b) Mn(1 mol/L)/$(Ce,La)CO_3F$.

three IR absorption peaks appeared on the catalyst surface at 1540 cm^{-1}, 1442 cm^{-1} and 1401 cm^{-1}. The absorption peak at 1540 cm^{-1} was attributed to the V_3 splitting pattern of bidentate nitrate, and the appearance of this peak was attributed to the oxidative adsorption of NH_3 by the oxygen species on the catalyst surface [40]. The absorption peaks at 1442 cm^{-1} and 1401 cm^{-1} belonged to NH_4^+ species on the Brønsted acidic sites [41] [42], which indicated that the synthetic $(Ce,La)CO_3F$ catalyst was relatively rich in acidic sites on the surface, but that these species were extremely unstable and decomposed and disappeared as the NH_3 influx time changed. Finally, the stability of the NH_3/ NH_4^+ species formed was observed by purging with N_2 for 30 min. It was found that after the N_2 purge, most of the NH_3/ NH_4^+ species formed on the catalyst surface disappeared, with only the dehydrogenation product eNH_2 produced by the NH_3 species at 1301 cm^{-1} remaining stable, and thus participated in the NH_3-SCR reaction. Notably, after N_2 purging, the catalyst showed a new IR absorption peak at 1518 cm^{-1}, where the peak was due to the dehydrogenation of -NH_2 species from NH_3 species adsorbed on the Brønsted acidic site [40].

Figure 7(b) showed the infrared spectrum of NH_3 adsorption with time for the Mn/$(Ce,La)CO_3F$ catalyst at 250˚C. From **Figure 7(b)**, it can be seen that when NH_3 was introduced for 5 min, infrared absorption peaks appeared on the catalyst surface at 1610 cm^{-1}, 1409 cm^{-1} and 1224 cm^{-1}, with the absorption peak at 1610 cm^{-1} attributed to the NH_3 species in the Lewis acidic site [41], and this species disappeared quickly with increasing time, which indicated its unstable adsorption. The absorption peaks at 1409 cm^{-1} and 1224 cm^{-1} are attributed to asymmetric bending vibrations occurring in the NH_4^+ species at the Brønsted acidic site [43] [44] and the NH_3 species at the Lewis acidic site, respectively. The

infrared absorption peak at 1653 cm^{-1} on the catalyst surface after 10 min of passage belongs to the NH_4^+ species at the Brønsted acidic site [45] [46]. This indicated that Mn/(Ce,La)CO_3F was dominated by Brønsted acidic sites on the catalyst surface at 250˚C, accompanied by a small amount of Lewis acidic sites to promote the reaction. This suggested that the use of manganese nitrate solution as a precursor could provide more Brønsted acidic sites for the catalyst. It has been reported in the literature that Brønsted acidic sites have a facilitative effect on the NH_3-SCR reaction [47], and after loading, the NH_3/ NH_4^+ species produced by NH_3 adsorption were more stable compared to (Ce,La)CO_3F. The species were present in a very stable state on the catalyst surface, both with increasing NH_3 influx time and N_2 purging, thus facilitating the NH_3-SCR reaction. In addition, the intensity of the absorption peaks of the species adsorbed on the Lewis and Brønsted acidic sites increased slightly, probably because the nitric acid caused some cracks on the catalyst surface, resulting in more oxygen vacancies on the catalyst surface, which facilitated the adsorption of Ce^{4+} on the acidic sites.

Compared to both catalysts, the NH_3/ NH_4^+ species formed on the surface of the Mn/(Ce,La)CO_3F catalyst are more stable and have more Brønsted acidic sites as well as oxygen vacancies, allowing more Ce^{4+} in the carrier to participate in the reaction in combination with the NH_3/ NH_4^+ species.

To further investigate the effect of catalysts on NO adsorption and activation performance, the in-situ infrared spectra of NO+O_2 adsorption with time for two different catalysts at the optimum denitrification temperature conditions were also investigated, as shown in **Figure 8**. **Figure 8(a)** showed the infrared spectrum of NO+O_2 adsorption with time for the synthetic (Ce,La)CO_3F catalyst at 200˚C. It can be found that (Ce,La)CO_3F showed two IR absorption peaks on

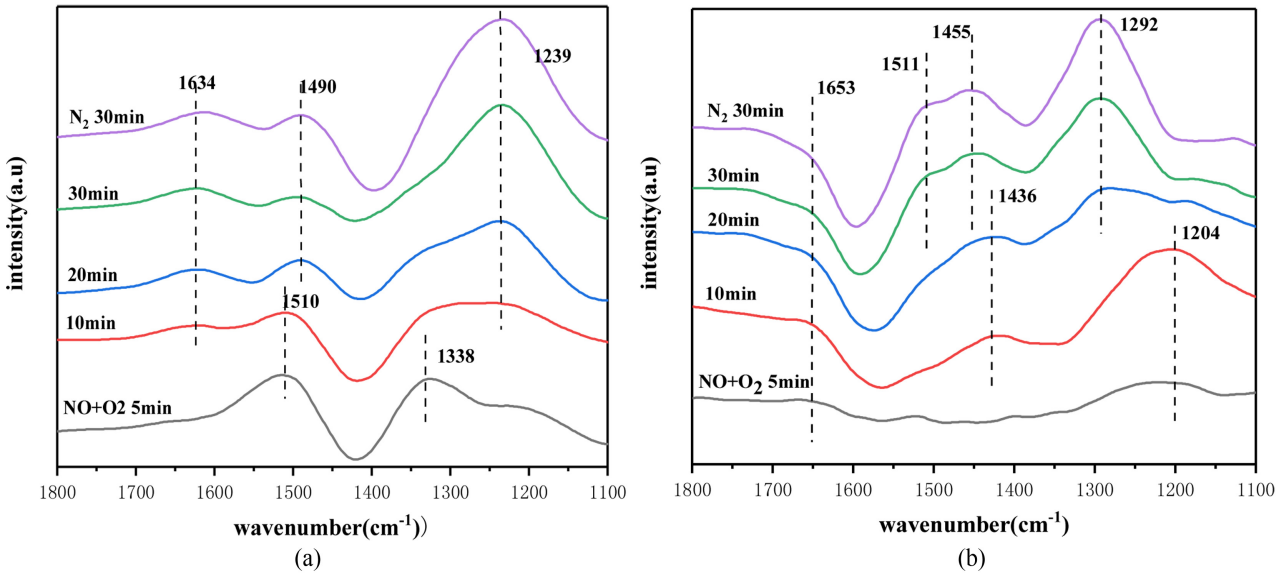

Figure 8. *In-situ* infrared spectra of NO+O_2 adsorption of the catalyst at the optimal denitration temperature over time. (a) (Ce,La)CO_3F. (b) Mn(1 mol/L)/(Ce,La)CO_3F.

the catalyst surface at 1510 cm^{-1} and 1338 cm^{-1} at 5 min of $NO+O_2$ pass, the absorption peak at 1510 cm^{-1} belonged to a monodentate nitrate species [48], and the absorption peak at 1338 cm^{-1} is attributed to a bidentate nitrate species [49], with the $NO+O_2$ passage time increased, the absorption peak of the bidentate nitrate species was found to disappear gradually, which indicated that its adsorption on the catalyst surface was less stable and prone to decomposition. The absorption peak of the monodentate nitrate species at 1510 cm^{-1} was shifted to 1490 cm^{-1} at 10 min of $NO+O_2$, where the nitrate species was still monodentate, probably due to the large amount of monodentate nitrate species produced during the reaction. At 10 min IR absorption peaks appeared at 1634 cm^{-1} and 1239 cm^{-1} on the catalyst surface, the absorption peak at 1634 cm^{-1} belonged to the bidentate nitrate species and weak adsorption could be found. The peak at 1239 cm^{-1} belonged to the bridging nitrate species [49] [50]. With increasing $NO+O_2$ influx time and final purging with N_2, the monodentate nitrate, bidentate nitrate and bridging nitrate species were all present on the catalyst surface in a very stable state.

Figure 8(b) showed the *in situ* IR spectra of $NO+O_2$ adsorption over time for the Mn/(Ce,La)CO_3F catalyst at 250˚C. From **Figure 8(b)**, it can be seen that there is no obvious large trend of IR absorption peaks on the catalyst surface when $NO+O_2$ is introduced for 5 min. With increasing $NO+O_2$ pass time, strong IR absorption peaks appeared on the catalyst surface at 1436 cm^{-1} and 1204 cm^{-1} at 10 min. The absorption peaks at 1436 cm^{-1} belonged to monodentate nitrate species, and the absorption peaks at 1204 cm^{-1} were attributed to nitrate species bound at the Mn-O-Ce site [51] [52], and similarly at 10 min, the absorption peak at 1653 cm^{-1} belonged to the bidentate nitrate species and the bidentate nitrate species was present in a very stable state as the $NO+O_2$ pass time increased. At 20 min, the IR absorption peaks at 1511 cm^{-1}, 1455 cm^{-1} and 1292 cm^{-1} on the catalyst surface were all attributed to the monodentate species [49] [53], and the monodentate species was very stable after N_2 purging. It is noteworthy that the number of monodentate nitrate species on the catalyst surface increased with Mn loading compared to the (Ce,La)CO_3F catalyst, with a new nitrate species (bridged nitrate) appearing at 1204 cm^{-1} at 10 min, so it can be judged that these nitrate species bonded to the Mn^{3+} provided by the loaded Mn to form intermediate products that participated in the SCR reaction. In addition, the absorption peak intensities of the monodentate nitrate species were also greatly increased by the loading of Mn.

In this experiment, the process of NH_3 adsorption and activation on the catalyst surface under different temperature conditions was investigated by *in situ* infrared spectroscopy for both catalysts, and the forms of NH_3 species present on the catalyst surface under different temperature conditions were studied. **Figure 9(a)** showed the spectrum of the change in thermal stability of the NH_3 adsorbed species of (Ce,La)CO_3F in the interval of 50˚C - 400˚C. Firstly, it can be observed that throughout the temperature interval, two distinct infrared absorption peaks appear on the catalyst surface at 1624 cm^{-1} and 1317 cm^{-1}. The absorption peak

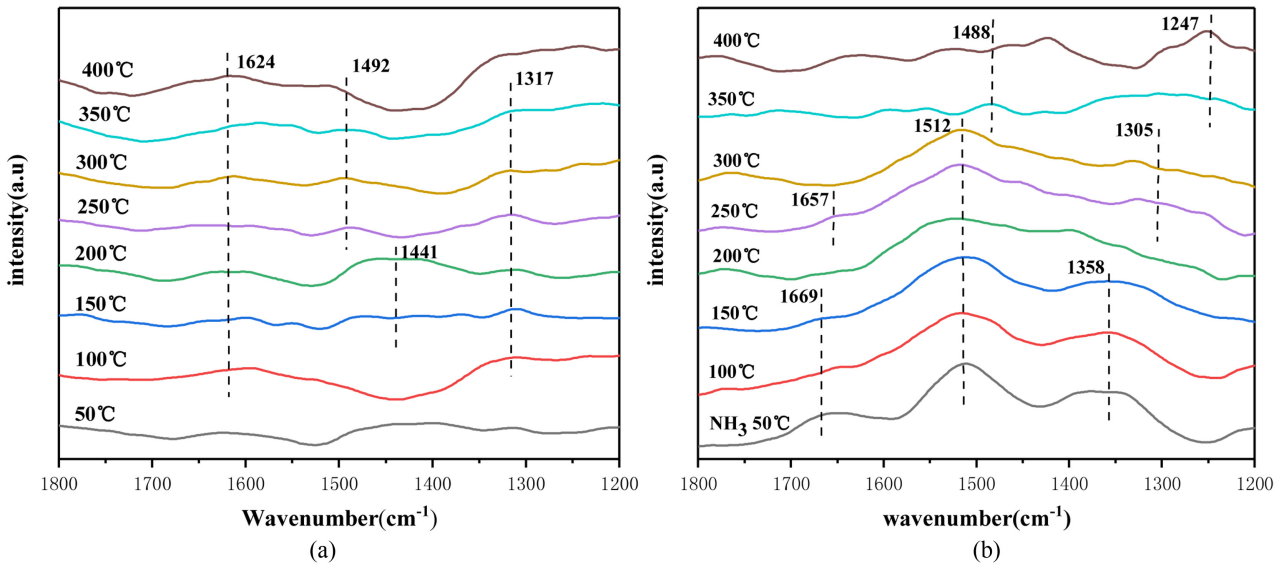

Figure 9. *In-situ* infrared spectra of NH_3 adsorbed species on the catalyst surface under different temperature conditions. (a) $(Ce,La)CO_3F$. (b) Mn(1 mol/L)/$(Ce,La)CO_3F$.

at 1624 cm^{-1} belonged to NH_2, an intermediate product of the dehydrogenation reaction of the NH_3 species at the Lewis acidic site [43]. The absorption peak at 1317 cm^{-1} belonged to the NH_4^+ species at the Brønsted acidic site [46], so it can be assumed that the Brønsted/Lewis acidic site is involved in the reaction throughout the temperature interval. It is noteworthy that in the range of 150˚C - 200˚C, an infrared absorption peak appeared on the catalyst surface at 1441 cm^{-1}, where the absorption peak belonged to the NH_4^+ species on the Brønsted acidic site [39], which indicated that more acidic sites were involved in the reaction in the range of 150˚C - 200˚C, with the Brønsted acidic site being the main acidic site, which favoured the catalytic reaction, which is consistent with the activity test results. As the temperature increased, the absorption peak at 1441 cm^{-1} was shifted to 1492 cm^{-1} and the intensity of the absorption peak was weakened, resulting in a decrease in denitrification efficiency. Overall, it appears that the $(Ce,La)CO_3F$ catalyst has a weak peak intensity throughout the reaction temperature range, which indicated that this catalyst has a poor adsorption capacity for NH_3, which is the reason for the low denitrification efficiency.

Figure 9(b) showed the variation of the thermal stability of the Mn/$(Ce,La)CO_3F$ catalyst for NH_3 adsorbed species in the interval 50˚C - 400˚C. From **Figure 9(b)**, it can be observed that a strong IR absorption peak at 1512 cm^{-1} appears on the catalyst surface in the temperature range of 50˚C - 300˚C. The absorption peak here is attributed to the amide ($-NH_2$) species produced by the dehydrogenation reaction of NH_4^+ species adsorbed on the Brønsted acidic site, in the temperature interval of 50˚C - 300˚C, the Brø nsted acidic sites play a major role, which also indicated that the manganese nitrate solution could provide more Brønsted acidic sites for the catalyst. It can also be observed that within the low temperature section (50˚C - 150˚C), infrared absorption peaks appear on the catalyst surface at 1669 cm^{-1} and 1358 cm^{-1}, with the absorption peak at 1669 cm^{-1} be-

longed to the NH_4^+ species on the Brønsted acidic site [44] and the absorption peak at 1358 cm^{-1} belonged to the deformation vibration of the N-H bond on the Brønsted acidic site. The Lewis acidic site was not detected throughout the low temperature section, which indicated that the Brønsted acidic site occupied the main active site in the low temperature section. With increasing temperature, only the amide (-NH_2) species at 1512 cm^{-1} was stable in the range of 200˚C - 300˚C. All other absorption peaks belonged to the Brønsted acidic site underwent pyrolysis and desorption, but were accompanied by the appearance of some new absorption peaks. The absorption peak at 1657 cm^{-1} belonged to the intermediate product $-NH_2$ species after dehydrogenation of NH_3, and the absorption peak at 1305 cm^{-1} belonged to the eNH_2 species generated by the dehydrogenation reaction of the activated NH_3 species [39]. According to the denitrification activity test results, it can be obtained that the denitrification rate decreases to a certain extent at 200˚C, and then there is a substantial recovery at 250˚C. From **Figure 9(b)**, it can be seen that the NH_4^+ species at 1358 cm^{-1} and 1669 cm^{-1} decompose when the reaction temperature reaches 200˚C, and only the amide (-NH_2) species at 1512 cm^{-1} is involved in the reaction on the catalyst surface, so causing such a phenomenon to occur.

The process of $NO+O_2$ species adsorption and activation on the catalyst surface under different temperature conditions was investigated by *in situ* infrared spectroscopy to discuss the forms and changes of NOx species present on the catalyst surface under different temperature conditions. **Figure 10(a)** showed the infrared variation spectrum of thermal stability of $NO+O_2$ adsorbed species on the (Ce,La)CO_3F catalyst in the temperature interval of 50˚C - 400˚C. Firstly, it can be observed that only one IR absorption peak appears on the catalyst surface at 1438 cm^{-1} in the temperature interval 50˚C - 100˚C. The absorption peak here can be attributed to the monodentate nitrate species [51], but as the temperature increases, the monodentate species decomposes, so it only occupies the

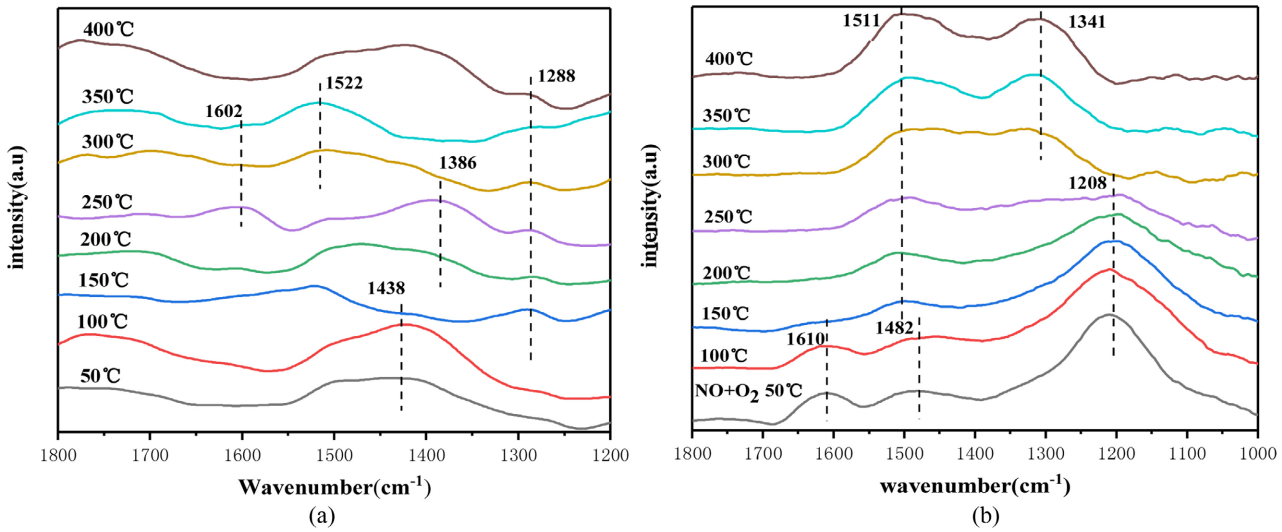

Figure 10. *In-situ* infrared spectra of $NO+O_2$ adsorbed species on the catalyst surface under different temperature conditions. (a) (Ce,La)CO_3F. (b) Mn(1 mol/L)/(Ce,La)CO_3F.

active site in the low temperature section. In the temperature interval of 150˚C - 250˚C, IR absorption peaks appeared on the catalyst surface at 1288 cm^{-1}, 1386 cm^{-1} and 1602 cm^{-1}. The absorption peaks at 1288 cm^{-1} and 1386 cm^{-1} both belonged to monodentate nitrate species [43] [49], and the IR absorption peak at 1602 cm^{-1} belonged to the Ce-O-Ce site on the NO_2 species [38]. It is clear that only some of the monodentate nitrate species are relatively more stable in this temperature interval, occupying the active sites in the middle and high temperature bands. As the temperature increased, the NO_2 species disappeared and a new monodentate nitrate species appeared at 1522 cm^{-1}. Throughout the temperature interval, the nitrate species produced by adsorbed NO were dominated by monodentate nitrate, but the adsorption and its instability and susceptibility to decomposition by temperature contributed to the poor denitrification activity.

Figure 10(b) showed the IR variation spectrum of the thermal stability of the $NO+O_2$ adsorbed species of the Mn/(Ce,La)CO_3F catalyst in the interval of 50˚C - 400˚C. As can be seen from **Figure 10(b)**, strong IR absorption peaks appear on the catalyst surface at 1208 cm^{-1}, 1482 cm^{-1} and 1610 cm^{-1} in the temperature interval of 50˚C - 250˚C. The absorption peaks at 1208 cm^{-1} and 1482 cm^{-1} belonged to the monodentate nitrate species formed on the Mn-O-Ce site [51]. The absorption peak at 1610 cm^{-1} belonged to NO_2 species adsorbed on the catalyst surface [45]. It has been reported in the literature that NO_2 species are important intermediates in the fast SCR reaction under low temperature conditions and also an important factor in improving the catalytic performance of the catalyst [54] [55] [56]. As the temperature continues to rise, the NO_2 species disappears, which indicates that it is less stable and prone to decomposition, while the monodentate nitrate species is relatively more stable. The absorption peak at 1511 cm^{-1} is a monodentate species formed by the shift of the absorption peak at 1482 cm^{-1}. The shift and increase in peak intensity is due to the gradual formation of more monodentate species on the catalyst surface, so that until 250˚C the monodentate species occupies the main active site in the reaction. As the temperature continues to increase, the peak of the monodentate nitrate species gradually disappears and a peak belonged to the bidentate nitrate species appears at 1341 cm^{-1}. The high temperature inactivation may be due to the fact that Mn^{3+} and Ce^{3+} only bond with the monodentate nitrate species to form O-Mn^{3+}-O-NO and O-Ce^{3+}-O-NO intermediates to participate in the reaction, and not with the other nitrate species. Compared to the synthetic (Ce,La)CO_3F catalyst, the loading of Mn resulted in the formation of a greater number of monodentate nitrates and a very significant increase in the peak intensity of the absorption peaks, which in turn bound transition metal ions to participate in the reaction. There is a reduction in the number of nitrate species on the catalyst surface, but an increase in the absorption peak intensity of the monodentate species, which occupies the active site throughout the denitration temperature band.

To further investigate the NH_3-SCR reaction mechanism of the catalyst, in-situ IR spectroscopy of the catalyst was carried out under different reaction conditions at the optimum denitrification temperature. **Figure 11(a)** showed the

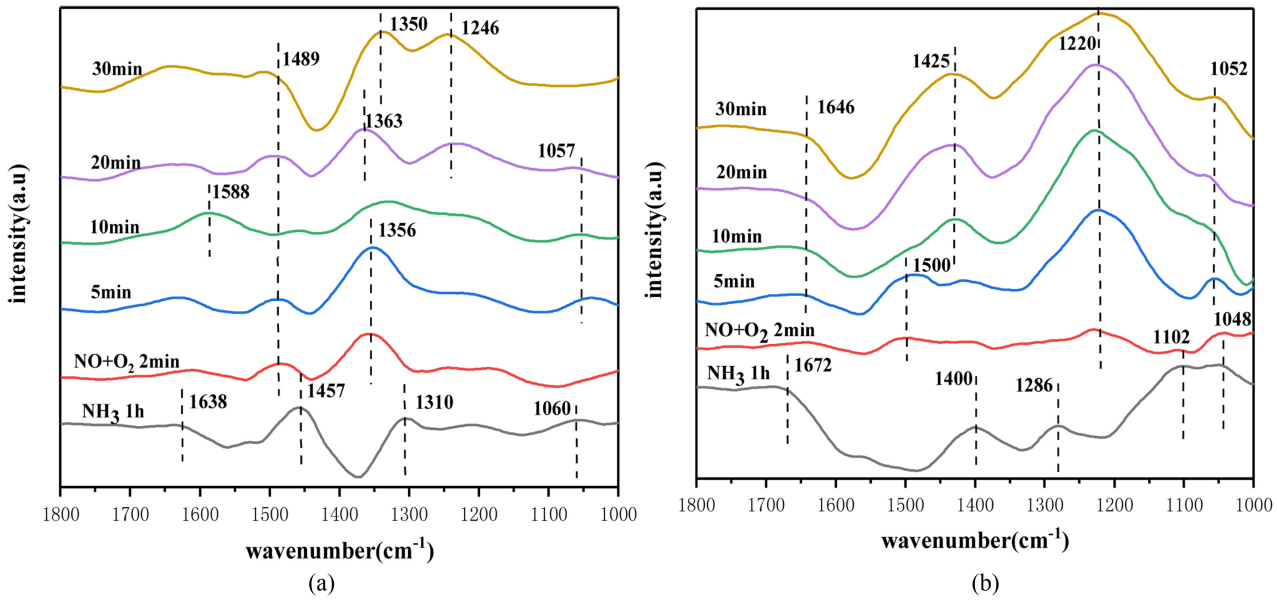

Figure 11. *In-situ* infrared spectra of the reaction of NH_3 pre-adsorbed species on the catalyst surface under the optimal reaction temperature.

in situ IR spectra of the reaction of $NO+O_2$ on the surface of the $(Ce,La)CO_3F$ catalyst with preadsorbed NH_3 species at 200˚C. The NH_3 gas was first introduced into the IR reaction cell containing the catalyst for 60 min, before which N_2 was used as a supplementary gas to pretreat the catalyst at 200˚C for 30 min, then the NH_3 gas was stopped and purged with N_2 for 10 min. The changes in the IR spectrum of the catalyst surface were observed at 200˚C. After first adsorption of NH_3 for 1 h, it can be found that more stable NH_3 adsorption species appear on the catalyst surface at 1638 cm^{-1}, 1457 cm^{-1}, 1310 cm^{-1} and 1060 cm^{-1}. The IR absorption peaks at 1638 cm^{-1} and 1060 cm^{-1} are attributed to NH_3 species on the Lewis acidic site [57], and the IR absorption peaks at 1457 cm^{-1} and 1310 cm^{-1} are attributed to NH_4^+ species on the Brønsted acidic site. NH_3 was switched off and $NO+O_2$ gas was then introduced into the reaction cell. When $NO+O_2$ was introduced for 2 min, the NH_4^+ species on the Brønsted acidic sites at 1457 cm^{-1} and 1310 cm^{-1} and the NH_3 species belonging to the Lewis acidic site at 1060 cm^{-1} disappeared rapidly, and only the absorption peak at 1638 cm^{-1} was present, which indicated that the NH_3/ NH_4^+ species could react rapidly with NO here. The E-R reaction mechanism exists on the surface of the $(Ce,La)CO_3F$ catalyst and the main reacting species are NH_3/ NH_4^+ species and NO species. With increasing $NO+O_2$ influx time, the infrared absorption peaks of NO adsorbed species appear at 1489 cm^{-1} and 1356 cm^{-1} on the catalyst surface at 5 min, both of which are monodentate nitrate species. At 10 min the absorption peaks of the monodentate nitrate species weakened, and according to the IR profiles of the $(Ce,La)CO_3F$ catalysts for $NO+O_2$ adsorption over time, the monodentate nitrate species were very stable over time, so the weakening of the monodentate nitrate here was probably due to the reaction with the incomplete-

ly reacted NH_3/ NH_4^+ species, which suggested that the L-H mechanism was also present here, with the main reacting species were NH_3/ NH_4^+ species and O-Ce^{3+}-O-NO species. With increasing time, many new spectral bands of nitrate species appeared on the catalyst surface. The IR absorption peaks at 1363 cm^{-1} and 1350 cm^{-1} belong to monodentate nitrate species adsorbed on the Ce-O-Ce sites on the catalyst surface, and the IR absorption peaks at 1588 cm^{-1} and 1246 cm^{-1} belonged to bridged nitrate species [58]. the peak at 1057 cm^{-1} belonged to the linked secondary nitrate species [$-(N_2O_2)^{2-}$] [59] [60].

Figure 11(b) showed the *in situ* IR spectra of the reaction of NO+O_2 on the surface of the Mn/(Ce,La)CO_3F catalyst with preadsorbed NH_3 species at 250˚C. When NH_3 was introduced into the reaction cell system for 60 min at 250˚C, IR absorption peaks could be observed on the catalyst surface at 1672 cm^{-1}, 1102 cm^{-1}, 1400 cm^{-1}, 1286 cm^{-1} and 1048 cm^{-1}, with the absorption peaks at 1672 cm^{-1} and 1048 cm^{-1} belonged to the NH_3 species at the Lewis acid site. The absorption peaks at 1102 cm^{-1}, 1400 cm^{-1} belonged to the NH_4^+ species at the Brønsted acid position and the absorption peak at 1286 cm^{-1} belonged to the e-NH_2 species generated by NH_4^+ dehydrogenation. With the passage of NO+O_2, the NH_3 adsorbed species all disappeared at 2 min, which indicated that NH_3/ NH_4^+ /e-NH_2 species can react with NO very quickly, so this catalyst surface follows the E-R mechanism. As the NO+O_2 pass time increased, nitrate species appeared on the Mn/(Ce,La)CO_3F catalyst surface at 5 min pass, with a bidentate nitrate species (1646 cm^{-1}), a monodentate nitrate species on the Mn-O-Ce site or the Ce-O-Ce site (1220 cm^{-1}), even a secondary nitrate [$-(N_2O_2)^{2-}$] (1052 cm^{-1}), and monodentate nitrate species (1500 cm^{-1}, 1425 cm^{-1}), but the disappearance of the absorption peak at 1500 cm^{-1} at 10 min was not due to a reaction with the NH_3 adsorbed species, but to the production of a large number of monodentate nitrate species causing the absorption peak at 1500 cm^{-1} to be shifted to 1425 cm^{-1}. This suggested that the Mn/(Ce,La)CO_3F catalyst followed the E-R mechanism at 250˚C with NH_3/ NH_4^+ /e-NH_2 and NO as the reacting species.

Figure 12 showed the in-situ IR spectra of the reaction of NH_3 with pre-adsorbed NO+O_2 species for both catalysts at optimum denitration temperature conditions. **Figure 12(a)** showed the transient in-situ IR spectrum of the (Ce,La)CO_3F catalyst at 200˚C temperature conditions. When NO+O_2 was introduced into the reaction cell system for 60 min, distinct IR absorption peaks appeared on the catalyst surface at 1618 cm^{-1}, 1489 cm^{-1}, 1340 cm^{-1} and 1252 cm^{-1}, with the absorption peaks at 1618 cm^{-1} attributed to NO_2 species (nitro or NO_2 molecules) adsorbed on the Ce-O-Ce sites. Monodentate nitrate species (1489 cm^{-1}), bidentate nitrate species (1340 cm^{-1}), and bridged nitrate species (1340 cm^{-1}) were also present, all of which were already present in a stable state on the catalyst surface. Turning off NO+O_2, NH_3 gas was then passed into the reaction cell. With the introduction of NH_3, it was observed that at 2 min the nitrate species generated on the surface of the (Ce,La)CO_3F catalyst disappeared and only the bridged nitrate species were present, but at 5 min they also participated in the reaction, which indicated that the NO_2 species, monodentate nitrate

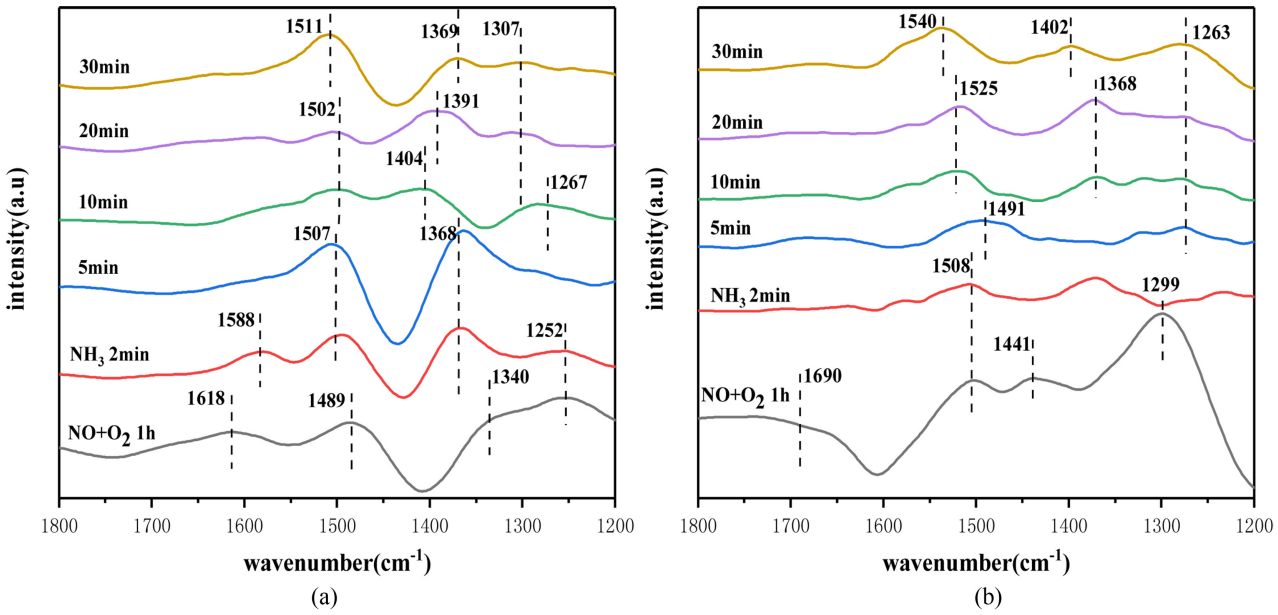

Figure 12. *In-situ* infrared spectra of the reaction of $NO+O_2$ pre-adsorbed species on the catalyst surface under the optimal reaction temperature. (a) $(Ce,La)CO_3F$. (b) Mn(1 mol/L)/$(Ce,La)CO_3F$.

and bridged nitrate species were involved in the reaction with the NH_3 adsorbed species. With increased NH_3 passage time, NH_4^+ species belonging to adsorbed on Brønsted acidic sites (1404 cm^{-1}, 1369 cm^{-1}, 1368 cm^{-1}, 1391 cm^{-1}) and NH_3 species belonging to Lewis acidic sites (1588 cm^{-1}, 1307 cm^{-1}, 1267 cm^{-1}) and amide species $-NH_2$ (1507 cm^{-1}, 1502 cm^{-1}, 1511 cm^{-1}) appeared on the catalyst surface, and the amide species $-NH_2$ (1507 cm^{-1}, 1502 cm^{-1}, 1511 cm^{-1}), which suggested that an L-H mechanism also exists on the surface of the $(Ce,La)CO_3F$ catalyst. The NH_3 species on the Lewis acidic site are less stable and prone to decomposition as can be seen from the graph. The absorption peaks of the monodentate nitrate species are the most intense among the adsorbed species of NO, so the main reactive species for the L-H mechanism are the NH_4^+ species on the Brønsted acidic site and the monodentate nitrate species bound to Ce^{3+}.

Figure 12(b) showed the *in situ* IR spectra of the reaction of NH_3 on the surface of the Mn/$(Ce,La)CO_3F$ catalyst with pre-adsorbed $NO+O_2$ species at 250˚C. When $NO+O_2$ was passed into the reaction cell system for 60 min at 250˚C, infrared absorption peaks could be observed on the catalyst surface at 1690 cm^{-1}, 1508 cm^{-1}, 1441 cm^{-1} and 1299 cm^{-1}, which belonged to the monodentate nitrate species (1508 cm^{-1}, 1299 cm^{-1}), the bidentate nitrate species (1690 cm^{-1}) and the trans $-N_2O_4$ cis $-N_2O_2$ species (1441 cm^{-1}), which decomposes NO due to the reduction of NO_2 by Ce^{3+}. When NH_3 was introduced, the absorption peaks of monodentate as well as bidentate nitrate species disappeared at 2 min, here in reaction with NH_3 adsorbed species, so that an L-H mechanism also existed on the Mn/$(Ce,La)CO_3F$ catalyst surface. With the passage of NH_3, NH_4^+ species belonged to the Brønsted acidic site (1402 cm^{-1}, 1491 cm^{-1}, 1525 cm^{-1}, 1508 cm^{-1}, 1540 cm^{-1}) and NH_3 species belonging to the Lewis acidic site (1368 cm^{-1},

1263 cm^{-1}) appear on the catalyst surface. It can be clearly seen that the Brønsted acidic sites on the catalyst surface are the most abundant and the NO adsorption species have the highest intensity of the monodentate nitrate absorption peak, so the main reactive species for the L-H mechanism are the NH_4^+ species and the O-Ce^{3+}-O-NO and O-Mn^{3+}-O-NO species.

The IR spectrum of the (Ce,La)CO_3F catalyst reveals E-R mechanism and L-H mechanism at an optimum denitrification temperature of 200˚C. The reactive species in the L-H mechanism are NH_4^+ species adsorbed on the Brønsted acidic site and monodentate nitrate species bonded to Ce^{3+}.

The reaction process of the L-H mechanism on the surface of the (Ce,La)CO_3F catalyst is as follows.

$$O_2 + 2* \rightarrow 2O^- * \quad (* \text{ NO adsorption sites on catalyst surfaces}) \tag{1}$$

$$NO + O_{2^-} * + Ce^{4+} = O \rightarrow \text{O-NO-O-}Ce^{3+} \quad \text{(monodentate nitrate)} \tag{2}$$

$$NH_3(g) \rightarrow NH_4^+(a) \quad \text{(Brønsted)} \tag{3}$$

$$Ce^{4+}\text{-}O^- + NH_4^+ \rightarrow Ce^{4+}\text{-}O^-\text{-}NH_3 + H^+ \rightarrow Ce^{4+}\text{-}O^-\text{-}NH_2 + 2H^+ \quad \text{(Brønsted)} \tag{4}$$

$$Ce^{4+}\text{-}O^-\text{-}NH_2 + \text{O-NO-O-}Ce^{3+} \rightarrow Ce^{4+}\text{-}O^-\text{-}NH_2\text{-O-NO-O-}Ce^{3+} \tag{5}$$

$$Ce^{4+}\text{-}O^-\text{-}NH_2\text{-O-NO-O-}Ce^{3+} \rightarrow Ce^{4+}\text{-}O^-\text{-}NH_2\text{-O-NO} + O{=}Ce^{4+} \tag{6}$$

$$Ce^{4+}\text{-}O^-\text{-}NH_2\text{-O-NO} \rightarrow N_2 + H_2O + Ce^{4+}\text{-}O^- \tag{7}$$

Mn/(Ce,La)CO_3F catalysts were subjected to E-R and L-H mechanisms at 250˚C. After loading with the transition metal Mn, the number of Brønsted acidic sites on the catalyst surface was increased, enhancing the ability to adsorb NH_3 on the catalyst surface. The number of nitrate species was relatively reduced, but the number and peak strength of monodentate nitrate increased, so that the main reacting species for the L-H mechanism of the Mn/(Ce,La)CO_3F catalyst were monodentate nitrate species bonded to the metal ions M^{n+} (Ce^{4+}, Mn^{4+}) and NH_4^+ species adsorbed on the Brønsted acidic sites. The reactions proceeded as follows. The L-H mechanism was shown in **Figure 13**.

$$O_2 + 2* \rightarrow 2O^- * \quad (* \text{ Newly introduced Mn provides NO adsorption site}) \tag{8}$$

$$NO + O_{2^-} * + M^{n+} = O \rightarrow \text{O-NO-O-}M^{(n-1)+} \quad \text{(monodentate nitrate)} \tag{9}$$

$$NH_3(g) \rightarrow NH_4^+(a) \quad \text{(Brønsted)} \tag{10}$$

$$Ce^{4+}\text{-}NH_4^+ + 2O^- \rightarrow Ce^{4+}\text{-}NH_2 + 2OH^- \quad \text{(Brønsted)} \tag{11}$$

$$Ce^{4+}\text{-}NH_2 + \text{O-NO-O-}M^{(n-1)+} \rightarrow Ce^{4+}\text{-}NH_2\text{-O-NO-O-}M^{(n-1)+} \tag{12}$$

$$Ce^{4+}\text{-}NH_2\text{-O-NO-O-}M^{(n-1)+} \rightarrow Ce^{4+}\text{-}NH_2\text{-O-NO} + O{=}M^{n+} \tag{13}$$

$$Ce^{4+}\text{-}NH_2\text{-O-NO} \rightarrow N_2 + H_2O + Ce^{4+}\text{-}O^- \tag{14}$$

The E-R reaction mechanism is also present on the surface of the (Ce,La)CO_3F catalyst at 200˚C. The reacting species are NO and NH_4^+ species at the Brønsted acidic site on the catalyst surface, and the E-R mechanism reaction

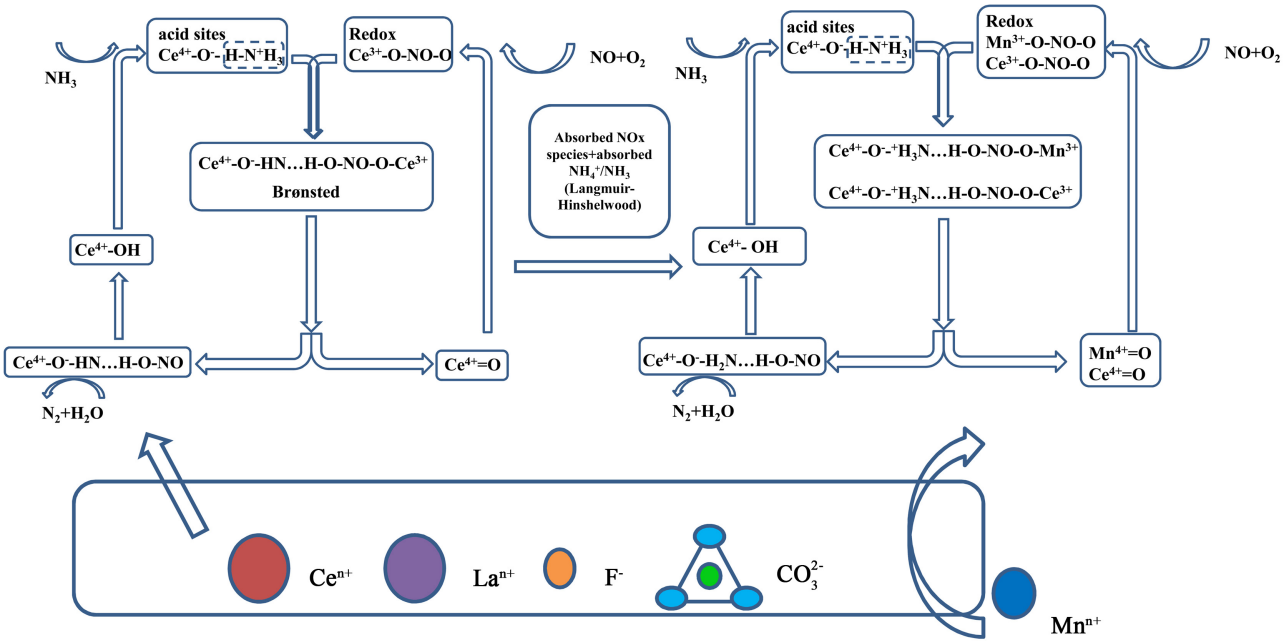

Figure 13. Schematic diagram of the L-H mechanism for the synthesis of (Ce,La)CO_3F and Mn-loaded catalysts.

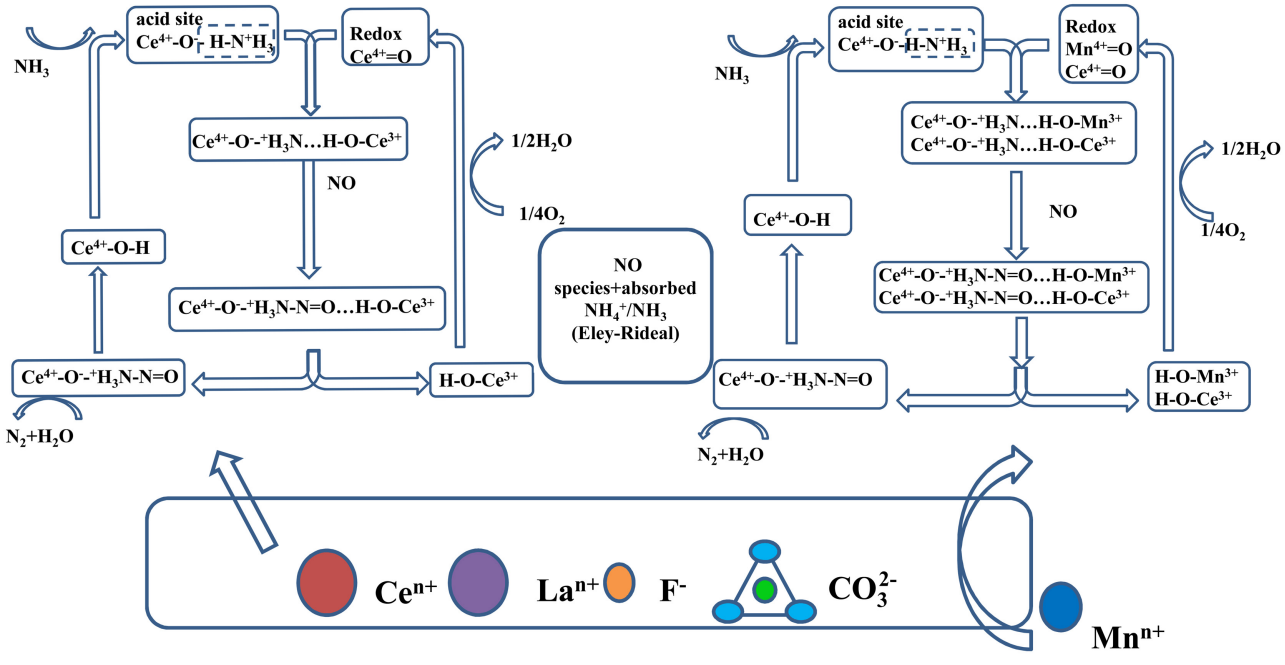

Figure 14. Schematic diagram of the E-R mechanism for the synthesis of (Ce,La)CO_3F and Mn-loaded catalysts.

proceeds as follows.

$$NH_3(g) \rightarrow NH_4^+(a) \quad \text{(Brønstedacidic sites)} \tag{15}$$

$$Ce^{4+}\text{-}O\text{-}NH_4^+ + Ce^{4+}=O \rightarrow Ce^{4+}\text{-}O^-\text{-}NH_3 + Ce^{3+}\text{-}OH \quad \text{(Brønsted)} \tag{16}$$

$$Ce^{4+}\text{-}O^-\text{-}NH_3^+\text{-}HO\text{-}Ce^{3+} + NO \rightarrow Ce^{4+}\text{-}O^-\text{-}NH_3^+\text{-}N{=}O\text{-}HO\text{-}Ce^{3+} \tag{17}$$

$$Ce^{4+}\text{-}O^-\text{-}NH_3^+\text{-}N{=}O\text{-}HO\text{-}Ce^{3+} \rightarrow Ce^{4+}\text{-}O^-\text{-}NH_3^+\text{-}N\text{-}O + HO\text{-}Ce^{3+} \tag{18}$$

$$Ce^{4+}\text{-}O^{-}\text{-}NH_3^{+}\text{-}N\text{-}O \rightarrow N_2 + H_2O + Ce^{4+}\text{-}OH \quad (19)$$

The Mn/(Ce,La)CO_3F catalyst also has an E-R mechanism at 250˚C. The reacting species are mainly NO and NH_4^+ species adsorbed on the acidic sites of Brønsted. The E-R mechanism reaction process of the Mn/(Ce,La)CO_3F catalyst is as follows, where M(Mn^{4+}, Ce^{4+}). The E-R mechanism was shown in **Figure 14**.

$$NH_3(g) \rightarrow NH_4^+(a) \quad \text{(Brønsted)} \quad (20)$$

$$Ce^{4+}\text{-}O\text{-}NH_4^+ + M^{n+}{=}O \rightarrow Ce^{4+}\text{-}O^{-}\text{-}NH_3^{+} + M^{(n-1)+}\text{-}OH \quad \text{(Brønsted)} \quad (21)$$

$$Ce^{4+}\text{-}O^{-}\text{-}NH_3 + NO \rightarrow N_2 + H_2O + Ce^{4+}\text{-}OH \quad (22)$$

$$M^{(n-1)+}\text{-}OH \rightarrow 1/4\,O_2 + 1/2\,H_2O + M^{n+}{=}O \quad (23)$$

5. Conclusion

In accordance with the cerium-lanthanum ratio of fluorocerium ores in the mineralogy of the Baiyun Ebo process, pure substances such as $Ce(NO_3)_3{\cdot}6H_2O$, $La(NO_3)_3{\cdot}6H_2O$ were used to synthesize (Ce,La)CO_3F grains to simulate bastnaesite minerals by hydrothermal method, and used as NH_3-SCR denitrification catalysts. After being roasted at a series of different temperatures, the catalyst surface produced a well-crystallised Ce_7O_{12} species as the active component for denitrification. The activity results showed that the synthetic (Ce,La)CO_3F was roasted at 500˚C, and the NOx conversion was 27% at 200˚C. The NH_3-SCR catalytic activity of the synthesised (Ce,La)CO_3F was improved by loaded transition metal Mn. The best catalyst was found to be produced by impregnating (Ce,La)CO_3F with 1 mol/L manganese nitrate solution, with a NOx conversion of 80% at 250˚C. The physicochemical properties were analysed using XRD, BET, H_2-TPR, NH_3-TPD and XPS. The loading of Mn resulted in the appearance of numerous well-dispersed MnOx species on the catalyst surface, the dispersion of Ce_7O_{12} species was also greatly enhanced, and the reduction in grain size indicated that Mn^{n+} entered into the (Ce,La)CO_3F lattice causing lattice shrinkage. The number of acidic sites on the catalyst surface and the redox capacity were enhanced. The amount of Ce^{3+} in the catalyst was also enhanced by the introduction of Mn^{n+}, but the proportion of adsorbed oxygen decreased, which indicated that the introduction of Mn^{n+} was detrimental to the increase in the proportion of adsorbed oxygen. The reaction mechanisms of the (Ce,La)CO_3F and Mn/(Ce,La)CO_3F catalysts were investigated by *in-situ* Fourier transform infrared spectroscopy (FTIR), to provide theoretical guidance for the specific reaction pathways of bastnaesite in the NH_3-SCR reaction. The results showed that catalysts followed both the E-R and L-H mechanisms throughout the reaction process. When loaded with Mn, the main reactive species in the L-H mechanism were the NH_4^+ (ad) species on the Brønsted acidic site and the O-Ce^{3+}-O-NO, O-Mn^{3+}-O-NO species. The main reactive species for the E-R mechanism were NH_3/ NH_4^+ (ad) species on the Brønsted/Lewis acidic sites and NO. The NH_4^+

(ad) species on the Brønsted acidic sites act as the main reactive NH_3(g) adsorbing species, bonded to the Ce^{4+} in the carrier (Ce,La)CO_3F to participate in the acid cycle reaction. The introduction of Mn^{n+} increases the number of Brønsted acidic sites on the catalyst surface, and acts as an adsorption site for NO, to react with NO to generate more monodentate nitrate species, to participate in the redox cycle reactions. The above results indicated that Mn^{n+} and (Ce,La)CO_3F have a good mutual promotion effect, which makes the loaded catalyst have excellent performance, which provides a theoretical basis for the high value utilization of bastnaesite.

Acknowledgements

This study was financially supported by Natural Science Foundation of Inner Mongolia (Grant No. 2019ZD13, 2020BS05030), National Natural Science Foundation of China (Grant No. 51866013). Thanks for Start-up Funds for Talent Introduction and Scientific Research of Institutions in Inner Mongolia Autonomous Region.

Conflicts of Interest

The authors declare no conflicts of interest regarding the publication of this paper.

References

[1] Zhu, Z.H., Yang, Z.F., Wang, Q.W., Wang, Z.J. and Li, N. (2019) Research on Process Mineralogy of Bayan Obo Rare Earth Concentrate. *Non-Ferrous Metals* (*Mineral Processing Part*), No. 6, 1-4+22.

[2] Huang, S.H., Wang, Z.G., Zhang, Z.M. and He, S.Y. (1986) Experimental Study on the Formation Conditions of Bastnaesite. *Acta Minera Sinica*, No. 2, 61-66.

[3] Mohammed, N., Kabbashi, N., Alade, A., *et al*. (2018) Advancement in the Utilization of Biomass-Derived Heterogeneous Catalysts in Biodiesel Production. *Green and Sustainable Chemistry*, **8**, 74-91. https://doi.org/10.4236/gsc.2018.81006

[4] Yao, X., Kong, T., Chen, L., *et al*. (2017) Enhanced Low-Temperature NH_3-SCR Performance of MnO_x/CeO_2 Catalysts by Optimal Solvent Effect. *Applied Surface Science*, **420**, 407-415. https://doi.org/10.1016/j.apsusc.2017.05.156

[5] Gong, P.J., Xie, J.L., Fang, D., He, F., Li, F.X. and Qi, K. (2020) Enhancement of the NH_3-SCR Property of Ce-Zr-Ti by Surface and Structure Modification with P. *Applied Surface Science*, **505**, Article ID: 144641. https://doi.org/10.1016/j.apsusc.2019.144641

[6] Li, J., Han, Y.X., Zhu, Y.H. and Zhou, R.X. (2011) Purification of Hydrogen from Carbon Monoxide for Fuel Cell Application over Modified Mesoporous CuO-CeO_2 Catalysts. *Applied Catalysis B*, *Environmental*, **108**-**109**, 72-80.

[7] Zhen, K.J. (2005) Fundamentals of Catalyst Action. Science Press, Beijing.

[8] Li, L.L. (2017) Preparation of Cerium-Based NH_3-SCR Catalyst and Its Denitrification Performance. Nanjing University, Nanjing.

[9] Zhang, K., Ge, Y., Zhu, J., *et al*. (2019) Surface Characteristics and Catalytic Activity of Modified Rare Earth Concentrate for Low-Temperature Selective Catalytic Re-

duction of NO_x with NH_3. *Materials Chemistry and Physics*, **2019**, Article ID: 122421. https://doi.org/10.1016/j.matchemphys.2019.122421

[10] Xie, S., Li, L., Jin, L., *et al*. (2019) Low Temperature High Activity of M (M = Ce, Fe, Co, Ni) Doped M-Mn/TiO_2 Catalysts for NH_3-SCR and *in Situ* DRIFTS for Investigating the Reaction Mechanism. *Applied Surface Science*, **515**, Article ID: 146014. https://doi.org/10.1016/j.apsusc.2020.146014

[11] Wang, X., Wu, S., Zou, W., *et al*. (2016) Fe-Mn/Al_2O_3 Catalysts for Low Temperature Selective Catalytic Reduction of NO with NH_3. *Chinese Journal of Catalysis*, **37**, 1314-1323. https://doi.org/10.1016/S1872-2067(15)61115-9

[12] Zhu, L. (2018) Study on the Performance and Mechanism of Low Temperature SCR Catalyst Denitrification with Transition Metal Oxides. Southeast University, Nanjing.

[13] Qiao, N.L., Yang, Y.X., Liu, Q.L., *et al*. (2018) Influence of Carrier Physicochemical Properties on the Denitrification Performance of NH_3-SCR with Manganese Cerium Catalysts. *Journal of Fuel Chemistry*, **46**, 733-742.

[14] Fang, D., Xie, J., Hu, H., *et al*. (2015) Identification of MnO_x Species and Mn Valence States in MnO_x/TiO_2 Catalysts for Low Temperature SCR. *Chemical Engineering Journal*, **271**, 23-30. https://doi.org/10.1016/j.cej.2015.02.072

[15] Tang, X., Li, Y., Huang, X., *et al*. (2006) MnOx-CeO_2 Mixed Oxide Catalysts for Complete Oxidation of Formaldehyde: Effect of Preparation Method and Calcination Temperature. *Applied Catalysis B*: *Environmental*, **62**, 265-273. https://doi.org/10.1016/j.apcatb.2005.08.004

[16] Wang, Z., Shen, G., Li, J., *et al*. (2013) Catalytic Removal of Benzene over CeO_2-MnO_x Composite Oxides Prepared by Hydrothermal Method. *Applied Catalysis B Environmental*, **s138**-**s139**, 253-259. https://doi.org/10.1016/j.apcatb.2013.02.030

[17] Chen, L., Yao, X., Cao, J., *et al*. (2019) Effect of Ti^{4+} and Sn^{4+} Co-Incorporation on the Catalytic Performance of CeO_2-MnO Catalyst for Low Temperature NH_3-SCR. *Applied Surface Science*, **476**, 283-292. https://doi.org/10.1016/j.apsusc.2019.01.095

[18] Zhang, L., Zou, W., Ma, K., *et al*. (2015) Sulfated Temperature Effects on the Catalytic Activity of CeO_2 in NH_3-Selective Catalytic Reduction Conditions. *The Journal of Physical Chemistry C*, **119**, 1155-1163. https://doi.org/10.1021/jp511282c

[19] Boningari, T., Ettireddy, P., Somogyvari, A., *et al*. (2015) Influence of Elevated Surface Texture Hydrated Titania on Ce-Doped Mn/TiO_2 Catalysts for the Low-Temperature SCR of NO_x under Oxygen-Rich conditions. *Journal of Catalysis*, **325**, 145-155. https://doi.org/10.1016/j.jcat.2015.03.002

[20] Geng, Y., Chen, X., Yang, S., *et al*. (2017) Promotional Effects of Ti on a CeO_2-MoO_3 Catalyst for the Selective Catalytic Reduction of NO_x with NH_3. *ACS Applied Materials & Interfaces*, **9**, 16951-16958. https://doi.org/10.1021/acsami.6b05380

[21] Kwon, D., *et al*. (2015) Influence of Tungsten on the Activity of a Mn/Ce/W/Ti Catalyst for the Selective Catalytic Reduction of NO with NH_3 at Low Temperatures. *Applied Catalysis A. General*, **497**, 160-166. https://doi.org/10.1016/j.apcata.2015.01.013

[22] Ma, H.Q., Tan, X. and Zhu, H.M. (2003) XPS Study of $La_{(1-x)}Ce_xFeO_3$ Chalcocite High-Conversion Catalysts. *Chinese Journal of Rare Earths*, No. 4, 445-448.

[23] Yang, J.M. and Su, M. (1992) Structure and Bond Properties of $Laga_{(1-x)}Fe_xO_3$. *Chinese Journal of Rare Earths*, No. 3.

[24] Yu, Y.L., Zhang, R.F., Liu, S.T., *et al*. (1992) XPS Study of $LaMn_{(1-x)}Co_xO_{(3-\lambda)}$ Catalysts. *Chinese Journal of Rare Earths*, No. 2, 134-137.

[25] Wang, J.S., Zhou, M.L., Zhang, J.X., *et al*. (2000) High-Temperature XPS Study of Carbonized La_2O_3-Mo Cathode Materials. *Journal of Materials Science and Engineering*, **29**, 225-227.

[26] Gnanakumar, E., Naik, M., Manikandan, M., *et al*. (2014) Gopinath, Role of Nanointerfaces in Cu- and Cu plus Au-Based Near-Ambient-Temperature CO Oxidation Catalysts. *ChemCatChem*, **6**, 3116-3124. https://doi.org/10.1002/cctc.201402581

[27] Zhao, K., Han, W., Lu, G.X., *et al*. (2016) Promotion of Redox and Stability Features of Doped Ce-W-Ti for NH_3-SCR Reaction over a Wide Temperature Range. *Applied Surface Science*, **379**, 316-322. https://doi.org/10.1016/j.apsusc.2016.04.090

[28] Xu, H., Xi, F., Shuang, L., *et al*. (2017) Promotional Effects of Titanium Additive on the Surface Properties, Active Sites and Catalytic Activity of $W/CeZrO_x$ Monolithic Catalyst for the Selective Catalytic Reduction of NO_x with NH_3. *Applied Surface Science*, **419**, 697-707. https://doi.org/10.1016/j.apsusc.2017.05.055

[29] Chang, L.H., Sasirekha, N., Chen, Y.W., *et al*. (2006) Preferential Oxidation of CO in H_2 Stream over Au/MnO_2-CeO_2 Catalysts. *Industrial & Engineering Chemistry Research*, **45**, 4927-4935. https://doi.org/10.1021/ie0514408

[30] Fan, J., Wu, X.D., Wu, X., *et al*. (2008) Thermal Ageing of Pt on Low-Surface-Area CeO_2-ZrO_2-La_2O_3 Mixed Oxides: Effect on the OSC Performance. *Applied Catalysis B Environmental*, **81**, 38-48. https://doi.org/10.1016/j.apcatb.2007.11.022

[31] Gao, Y., Luan, T., Zhang, S., *et al*. (2019) Comprehensive Comparison between Nanocatalysts of Mn-Co/TiO_2 and Mn-Fe/TiO_2 for NO Catalytic Conversion: An Insight from Nanostructure, Performance, Kinetics, and Thermodynamics. *Catalysts*, **9**, 175. https://doi.org/10.3390/catal9020175

[32] Gao, F., Tang, X., Yi, H., *et al*. (2017) *In-Situ* DRIFTS for the Mechanistic Studies of NO Oxidation over α-MnO_2, β-MnO_2 and γ-MnO_2 Catalysts. *Chemical Engineering Journal*, **322**, 525-537. https://doi.org/10.1016/j.cej.2017.04.006

[33] Kapteijn, F., Singoredjo, L., Andreini, A., *et al*. (1994) Activity and Selectivity of Pure Manganese Oxides in the Selective Catalytic Reduction of Nitric Oxide with a Mmonia. *Applied Catalysis B*: *Environmental*, **3**, 173-189. https://doi.org/10.1016/0926-3373(93)E0034-9

[34] Luo, S., Zhou, W., Xie, A., *et al*. (2016) Effect of MnO_2 Polymorphs Structure on the Selective Catalytic Reduction of NO_x with NH_3 over TiO_2-Palygorskite. *Chemical Engineering*, **286**, 291-299. https://doi.org/10.1016/j.cej.2015.10.079

[35] Huang, J., Huang, H., Jiang, H., *et al*. (2018) The Promotional Role of Nd on Mn/TiO_2 Catalyst for the Low-Temperature NH_3-SCR of NO_x. *Catalysis Today*, **332**, 49-58. https://doi.org/10.1016/j.cattod.2018.07.031

[36] Sun, P., Huang, S., Guo, R., *et al*. (2018) The Enhanced SCR Performance and SO_2 Resistance of Mn/TiO_2 Catalyst by the Modification with Nb: A Mechanistic Study. *Applied Surface Science*, **447**, 479-488. https://doi.org/10.1016/j.apsusc.2018.03.245

[37] Xu, Q., Su, R., Cao, L., *et al*. (2017) Facile Preparation of High-Performance Fe-Doped Ce-Mn/TiO_2 Catalysts for the Low-Temperature Selective Catalytic Reduction of NO_x with NH_3. *RSC Advances*, **7**, 48785-48792. https://doi.org/10.1039/C7RA07854D

[38] Li, Q., Gu, H., Li, P., *et al*. (2014) *In Situ* IR Studies of Selective Catalytic Reduction of NO with NH_3 on Ce-Ti Amorphous Oxides. *Chinese Journal of Catalysis*, **35**, 1289-1298. https://doi.org/10.1016/S1872-2067(14)60154-6

[39] Liu, H., Fan, Z., Sun, C., *et al*. (2019) Improved Activity and Significant SO_2 Tolerance of Samarium Modified CeO_2-TiO_2 Catalyst for NO Selective Catalytic Reduction with NH_3. *Applied Catalysis B*: *Environmental*, **244**, 671-683. https://doi.org/10.1016/j.apcatb.2018.12.001

[40] Yao, X., Zhao, R., Chen, L., *et al*. (2017) Selective Catalytic Reduction of NO_x by NH_3 over CeO_2 Supported on TiO_2: Comparison of Anatase, Brookite, and Rutile. *Applied Catalysis B*: *Environmental*, **208**, 82-93. https://doi.org/10.1016/j.apcatb.2017.02.060

[41] Sun, J., Lu, Y., Zhang, L., *et al*. (2017) Comparative Study of Different Doped Metal Cations on the Reduction, Acidity, and Activity of $Fe_9M_1O_x$ (M = Ti^{4+}, $Ce^{4+/3+}$, Al^{3+}) Catalysts for NH_3-SCR Reaction. *Industrial & Engineering Chemistry Research*, **56**, 12101-12110. https://doi.org/10.1021/acs.iecr.7b03080

[42] Liu, Y., Gu, T., Weng, X., *et al*. (2012) DRIFT Studies on the Selectivity Promotion Mechanism of Ca-Modified Ce-Mn/TiO_2 Catalysts for Low-Temperature NO Reduction with NH_3. *The Journal of Physical Chemistry C*, **116**, 16582-16592. https://doi.org/10.1021/jp304390e

[43] Liao, Y.J., Zhang, Y.P., Yu, Y.X., *et al*. (2016) *In Situ* Infrared Study of the Mechanism of Low-Temperature Selective Catalytic NO_x Reduction by MnO_x/WO_3/TiO_2. *Journal of Chemical Engineering*, **67**, 5033-5037.

[44] Topsoe, N.Y. (1994) Mechanism of the Selective Catalytic Reduction of Nitric Oxide by A Mmonia Elucidated by *in Situ* On-Line Fourier Transform Infrared Spectroscopy. *Science*, **265**, 1217-1219. https://doi.org/10.1126/science.265.5176.1217

[45] Chen, L., *et al*. (2010) DRIFT Study on Cerium-Tungsten/Titania Catalyst for Selective Catalytic Reduction of NO_x with NH_3. *Environmental Science & Technology*, **44**, 9590-9596. https://doi.org/10.1021/es102692b

[46] Peña, D., Uphade, B., Reddy, E., *et al*. (2004) Identification of Surface Species on Titania-Supported Manganese, Chromium, and Copper Oxide Low-Temperature SCR Catalysts. *The Journal of Physical Chemistry B*, **108**, 9927-9936. https://doi.org/10.1021/jp0313122

[47] Borfecchia, E., *et al*. (2015) Revisiting the Nature of Cu Sites in the Activated Cu-SSZ-13 Catalyst for SCR Reaction. *Chemical Science*, **6**, 548-563. https://doi.org/10.1039/C4SC02907K

[48] Yao, X., Chen, L., Cao, J., *et al*. (2019) Enhancing the deNO Performance of MnO/CeO_2-ZrO_2 Nanorod Catalyst for Low-Temperature NH_3-SCR by TiO_2 Modification. *Chemical Engineering Journal*, **369**, 46-56. https://doi.org/10.1016/j.cej.2019.03.052

[49] Sun, C., Liu, H., Chen, W., *et al*. (2018) Insights into the Sm/Zr Co-Doping Effects on N_2 Selectivity and SO_2 Resistance of a MnO_x-TiO_2 Catalyst for the NH_3-SCR Reaction. *Chemical Engineering*, **347**, 27-40. https://doi.org/10.1016/j.cej.2018.04.029

[50] Li, L., Wu, Y., Hou, X., *et al*. (2019) Investigation of Two-Phase Intergrowth and Coexistence in Mn-Ce-Ti-O Catalysts for the Selective Catalytic Reduction of NO with NH_3: Structure-Activity Relationship and Reaction Mechanism, *Industrial & Engineering Chemistry Research*, **58**, 849-862. https://doi.org/10.1021/acs.iecr.8b05066

[51] Song, L., Zhang, R., Zang, S., *et al*. (2017) Activity of Selective Catalytic Reduction of NO over V_2O_5/TiO_2 Catalysts Preferentially Exposed Anatase 001 and 101 Facets. *Catalysis Letters*, **147**, 934-945. https://doi.org/10.1007/s10562-017-1989-5

[52] Li, L., Tan, W., Wei, X., *et al*. (2018) Mo Doping as an Effective Strategy to Boost

Low Temperature NH_3-SCR Performance of CeO_2/TiO_2 Catalysts. *Catalysis Communications*, **114**, 10-14. https://doi.org/10.1016/j.catcom.2018.05.015

[53] Bendrjch, M., Scheuer, A., Hayes, R., *et al*. (2018) Unified Mechanistic Model for Standard SCR, Fast SCR, and NO_2 SCR over a Copper Chabazite Catalyst. *Applied Catalysis B*: *Environmental*, **222**, 76-87. https://doi.org/10.1016/j.apcatb.2017.09.069

[54] Sun, D., Liu, Q., Liu, Z., *et al*. (2009) Adsorption and Oxidation of NH_3 over V_2O_5/AC Surface. *Applied Catalysis B Environmental*, **92**, 462-467. https://doi.org/10.1016/j.apcatb.2009.09.005

[55] Gianguido, R. and Angeles, L. (2004) An FT-IR Study of the Adsorption and Oxidation of N-Containing Compounds over Fe_2O_3/Al_2O_3 SCR Catalysts. *Journal of Molecular Catalysis A Chemical*, No. 1, 215. https://doi.org/10.1016/j.molcata.2004.01.016

[56] Shan, Y., Shi, X., He, G., *et al*. (2018) Effects of NO_2 Addition on the NH_3-SCR over Small-Pore Cu-SSZ-13 Zeolites with Varying Cu Loading. *The Journal of Physical Chemistry C*, **122**, 25948-25953. https://doi.org/10.1021/acs.jpcc.8b05930

[57] Li, L., Zhang, F., Guan, N., *et al*. (2007) Selective Catalytic Reduction of NO by Propane in Excess Oxygen over IrCu-ZSM-5 Catalyst. *Catalysis Communications*, **8**, 583-588. https://doi.org/10.1016/j.catcom.2006.08.013

[58] Mihaylov, M., Ivanova, E., Aleksandrov, H., *et al*. (2015) FTIR and Density Functional Study of NO Interaction with Reduced Ceria: Identification of N_3 and NO_2 as New Intermediates in NO Conversion. *Applied Catalysis B*: *Environmental*, **s176-s177**, 107-119. https://doi.org/10.1016/j.apcatb.2015.03.054

[59] Mu, J., Li, X., Sun, W., *et al*. (2018) An Inductive Effect Boosting Catalytic Performance of Advanced Fei-xV_xO_6 Catalysts in Low-Temperature NH_3-SCR: An Insight into the Structure, Interaction, and Mechanisms. *ACS Catalysis*, **8**, 6760-6774. https://doi.org/10.1021/acscatal.8b01196

[60] Zhu, L., Zhong, Z., Yang, H., *et al*. (2017) $DeNO_x$ Performance and Characteristic Study for Transition Metals Doped Iron Based Catalysts. *Korean Journal of Chemical Engineering*, **34**, 1229-1237. https://doi.org/10.1007/s11814-016-0369-y